Univerzita Karlova v Praze
Matematicko-fyzikální fakulta

DIPLOMOVÁ PRÁCE

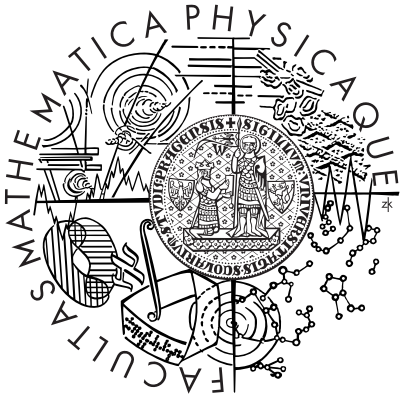

Miroslav Frost

Studium tepelných vlastností tvarově paměťových slitin na bázi NiMnGa

Katedra fyziky kondenzovaných látek

Vedoucí diplomové práce: Mgr. Alexandra Rudajevová, CSc.

Studijní program: Fyzika kondenzovaných soustav a materiálů

2008

Děkuji především své školitelce, Mgr. Alexandře Rudajevové, CSc., za všestrannou pomoc při vypracování mé diplomové práce, Dr. rer. nat. Robertu Královi, Dr. za pomoc s deformačními zkouškami a RNDr. Aleši Jägerovi, Ph.D. za poskytnutí strukturních fotografií a informací o výrobě vzorků.

Rád bych též poděkoval své rodině a přátelům za podporu při sepisování této práce.

Prohlašuji, že jsem svou diplomovou práci napsal samostatně a výhradně s použitím citovaných pramenů. Souhlasím se zapůjčováním práce.

V Praze dne 18. dubna 2008 Miroslav Frost

Contents

Abstract

Název práce: Studium tepelných vlastností tvarově paměťových slitin na bázi NiMnGa
Autor: Miroslav Frost
Katedra: Katedra fyziky kondenzovaných látek
Vedoucí diplomové práce: Mgr. Alexandra Rudajevová, CSc.
E-mail vedoucí: rud@mag.cuni.cz

Abstrakt: Teplotní závislost relativního prodloužení (RE) a koeficientu teplotní délkové roztažnosti (CTE) nedeformovaných a tlakem deformovaných polykrystalů slitiny $Ni_{53.6}Mn_{27.1}Ga_{19.3}$ s kolumnárními zrny byla studována v teplotním intervalu 300–650 K. Tato slitina patří mezi magnetické slitiny s tvarovou pamětí.

Pro nedeformovanou slitinu bylo vysvětleno rozšiřování hysterezní smyčky RE a posun transformačních píků CTE s rostoucí rychlostí ohřevu/chlazení.

Po deformaci slitiny byl pozorován jednocestný a dvoucestný paměťový jev a byla diskutována jejich souvislost s dalšími mechanickými vlastnostmi vzorku. Posun transformačních píků CTE při ohřevu slitiny byl spojen s vnitřním napětím vzniklým deformací. Hodnota vnitřního napětí byla spojena s hodnotou maximálního deformačního napětí. Za tohoto přepokladu byla z Clausiovy-Clapeyronovy rovnice odhadnuta hodnota kritického transformačního sklonu.

Na základě měření teplotní vodivosti byla určena tepelná vodivost studované slitiny v teplotním intervalu 300–650 K.

Klíčová slova: Jevy tvarové paměti, Ni-Mn-Ga, Dilatometrie, Deformace

Title: Study of the thermal properties of the shape memory NiMnGa based alloys

Author: Miroslav Frost
Department: Department of Condensed Matter Physics
Supervisor: Mgr. Alexandra Rudajevová, CSc.
Supervisor's e-mail address: rud@mag.cuni.cz

Abstract: The temperature dependence of the relative elongation (RE) and the linear coefficient of thermal expansion (CTE) of undeformed and compression pre-deformed polycrystals of $Ni_{53.6}Mn_{27.1}Ga_{19.3}$ alloy with columnar grains were studied in the temperature range 300–650 K. The Ni-Mn-Ga alloy belongs to magnetic shape memory alloys.

An artificial widening of the hysteresis loop of RE and a shift of transformation peaks in CTE for undeformed alloy due to increasing heating/cooling rate were explained.

The one-way shape memory effect and the two-way shape memory effect were observed after deformation of the alloy and their relation to other mechanical characteristics was discussed. A shift of transformation peaks of CTE after deformation was related to deformation imposed internal stress. The value of this stress was assumed to be related to the maximum deformation stress and the critical transformation slope of the Clausius-Clapeyron equation was estimated.

The thermal diffusivity of the studied alloy was measured by the flash method in the temperature range 300–650 K. Based on these results, the thermal conductivity of the alloy was determined.

Keywords: Shape Memory Effects, Ni-Mn-Ga, Dilatometry, Deformation

Preface

The shape memory alloys are intermetallics which exhibit the unique shape memory effect properties (*e.g.* superelasticity, one-way shape memory effect) based on the first-order solid-to-solid diffusionless martensitic phase transition. Among them, Ni-Mn-Ga based magnetic alloys are of particular interest for their giant magnetic shape memory effect, good technological properties and reasonable price. The increasing number of investigations of Ni-Mn-Ga based magnetic alloys in the last decade reflects growing global interest in these materials, which are promising from the wide range of possible applications point of view.

With respect to industrial applicability of Ni-Mn-Ga based alloys polycrystals could be a good alternative to single crystals. Unfortunately, polycrystals usually exhibit lower strains due to the presence of several inner fixed interfaces (*e.g.* grain boundaries) and different orientations of the separate crystals which affect the overall mechanical response. A possible approach to improve the material response of them is to impart a texture.

Significant structural changes related to martensitic phase transition are induced by thermal or mechanical loading in the shape memory alloys. Dilatometry is a useful method for research on processes connected with thermal loading, since it detects all length changes related to the change of temperature. An analysis of dilatometric characteristics, *e.g.* the relative elongation or the linear coefficient of thermal expansion (CTE), is a valuable source of information about the internal physical processes in materials.

The results of the research on the thermal properties of material, *e.g.* determination of the CTE or the thermal conductivity coefficient, are also of high technological relevance for both material processing (casting, annealing) and optimal functional properties development.

Since the shape memory alloys are usually concerned to work in combined mechanical and thermal loading cycles, the main aim of this thesis is to measure and analyze the RE and the CTE of $Ni_{53.6}Mn_{27.1}Ga_{19.3}$ alloy undergone a pre-deformation in compression. The results are also compared with measurements performed on the undeformed alloy of the same chemical composition. The second aim is to examine the influence of heating/cooling rate to dilatation characteristics of the undeformed alloy. Determination of the coefficient of thermal conductivity of the studied alloy is the last aim of this thesis.

In the first chapter of this thesis the martensitic phase transition is introduced and shape memory effects extensively described. Some specific properties of Ni-Mn-Ga based alloys are also mentioned. In the second chapter the experimental methods and equipment are described. In the third and fourth chapters the results of experiments are described and discussed. In the last chapter conclusions of this thesis can be found.

1 Introduction

1.1 Martensitic Phase Transformation

Intermetallic alloys exhibiting the unique shape memory effects (SMEs) are known as shape memory alloys (SMAs). Although these effects were firstly observed at Au-Cd alloy in 1951, the research has intensified after 1963, when the commercially most successful Ni-Ti-based shape memory alloys were discovered.

The key physical process for understanding of all shape memory effects, which are described in more detail in the next section, is the *martensitic phase transition* (MT). This first-order solid-to-solid phase transition from the parent phase, which is referred to as *austenite*, to the less-ordered product phase, *martensite*, is a typical example of so-called *military transition*. The mechanism of this type of transformation consists of a regular rearrangement of the lattice in such way that relative displacement of neighboring atoms does not exceed the interatomic distances and the atoms do not interchange places. This "shearing of the parent lattice into the product" is sometimes referred as *lattice-distortive* transition. The name emphasizes the analogy between the coordinated motion of atoms crossing the glissile interface between the parent and product phases and that of soldiers moving in ranks on the parade ground. (In contrast, the uncoordinated transfer of atoms across a non-glissile interface results in what is known as a civilian transformation.) That is why the interface between austenitic and martensitic phases reaches almost the speed of sound in the solid.

In most cases, the martensitic transformation is nucleated heterogeneously by formation of thin plates of parent/product phase in the matrix of product/parent phase, at special defect sites in a SMA material, forming a two-phase austenite-martensite zone. The defects induce a strain field that facilitates the initiation of the transformation (lowers the energy barrier for nucleation). In a SMA polycrystalline body, the mechanism of martensite phase transformation is complicated by interaction of the walls of growing or shrinking martensite plates with the grain boundaries of the austenite matrix. The two principles determining MT were established by Kurdjumov [1]:

1. A martensitic transformation is a strain transformation, i.e. the lattice strain (also called self-strain) is a transformation parameter which determines physical state of an initial phase and a product phase. The self-strain in a more general case can include, in addition to the homogeneous strain, some kind of rearrangement or shuffling of lattice sites, provided that this shuffling is unambiguously related to the strain. (The free energy as a function of an uniform transformation strain is then a primary quantitative characteristic of martensitic transition determining its thermodynamics and kinetics.)

2. The coherency of a two-phase structure determines its evolution from an initial phase to a product phase.

Let us recall here the first-order phase transitions exhibit a discontinuity in the first derivative of the thermodynamic potential (e.g. free energy) with respect to the thermodynamic variable, e.g. a discontinuity in strain, in entropy (which is connected with the latent heat), etc.

In general, the martensitic transformation is *diffusionless* and *athermal*. It means the amount of martensite formed is a function only of the temperature and not of the length of time at which the alloy is held at that temperature. Athermal transformations start at well-defined temperatures, which are usually insensitive to rate-effects. Furthermore, in the case of SMA the MT is *thermoelastic* (in contrast to ferrous materials), which indicates:

1. The thermodynamic driving force for the phase transformation is rather small.
2. The domain walls are very mobile (small internal friction) and their motion is reversible.
3. The product phase stays coherent with the parent phase (the displacement field is continuous).

These properties imply that no plastic flow is generated during the transformation, the transformation is fully reversible – therefore SMA products can undergo a great number of transformation cycles almost without any fatigue – and dissipation of energy during transformation is quite small. Energy dissipation, although small, is responsible for *hysteretic properties* of SMA and therefore plays an important role in the process of transformation. The essential contributions to the energy dissipation are associated with interfacial friction, defect production and acoustic emission caused by nucleation and growth of martensite plates and interactions between them during transformation [2]. Further metallurgical aspects of MT (as detailed description of martensite nucleation and growth or stabilization) can be found, for instance, in [3].

The MT can be driven by temperature or by changing external stresses or by simultaneous change of stresses and temperature. The temperature induced transformation proceeds by formation, expansion and migration of a two-phase zone from cooled or heated boundaries. In a SMA polycrystalline body the stress induced transformation can be driven by shear loading or by tension or compression, since even a simple uniaxial loading induces a complex 3-D microstress field with nonzero shear component in individual grains of polycrystalline body due to its inhomogeneous structure. The shift of the two-phase equilibrium under stress results not only in the change of quantity of a martensite phase but also in the change of the variant fractions in it.

If there is no preferred direction for the occurrence of the transformation, the martensite takes advantage of the existence of different possible ordering, forming a series of crystallographically equivalent variants. The product phase growing to

a platelet shape is then termed *multiple-variant martensite* and is characterized by a twinned microstructure, which minimizes the misfit between the martensite and surrounding austenite. On the other hand, if there is a preferred direction for the occurrence of transformation (e.g. imposed stress), all the martensitic crystals tend to be formed to the most favorable variant. The product phase is termed *fully oriented martensite*[1] and is characterized by a *detwinned* structure, which again minimizes the misfit between the martensite and the surrounding austenite. Moreover, the conversion of each variant of martensite into different single variant is possible. Such process is known as *reorientation process*. Two effects determine the change of the martensitic variants fraction during stress induced processes:

- selection of martensite plates with preferable orientation with respect to the external stress,
- increase of fraction of the preferable variants in a martensite plates.

From a crystallographic point of view, in general SMA parent phases have super-lattice body-centered cubic structures and are classified as β-phase alloys. The martensite crystals obtained from β-phase austenite are indicated as β' and have periodic stacking order structures. Since in the martensite atoms of different radii are packed without any symmetry, the super-lattice structure tends to deform slightly, resulting in a typical monoclinic configuration. Depending on alloy, upon cooling and before the formation of martensite slight crystallographic changes (*e.g.* a small lattice distortion) might be observed. These intermediate states are often termed *pre-martensitic phases*. In some SMAs, structure of the martensitic lattice can slightly change when changing temperature or stress which leads to forming *intermartensitic phases*. Usually, the maximum amount of recoverable strain and the hysteresis loop in these cases are small compared to the ones associated with the full martensitic transition.

In the last decade a new class of SMAs was developed and intensively studied. They are called *magnetic shape memory alloys* (MSMAs) or ferromagnetic shape memory alloys since MT can be induced by temperature, stress and even external magnetic field change [4]. The result of MT in a sigle crystal is a giant magnetic field-induced strain (MFIS). It is based on the rearrangement of martensite twin variants under a magnetic field. The crystal structure basis for the occurrence of MFIS is high magnetic anisotropy of the martensitic phase, in which exists only one easy magnetization axis. Martensite variants that have their easy axis along the applied field direction grow at the expense of other variants by twin boundary motion driven by the applied field [5].

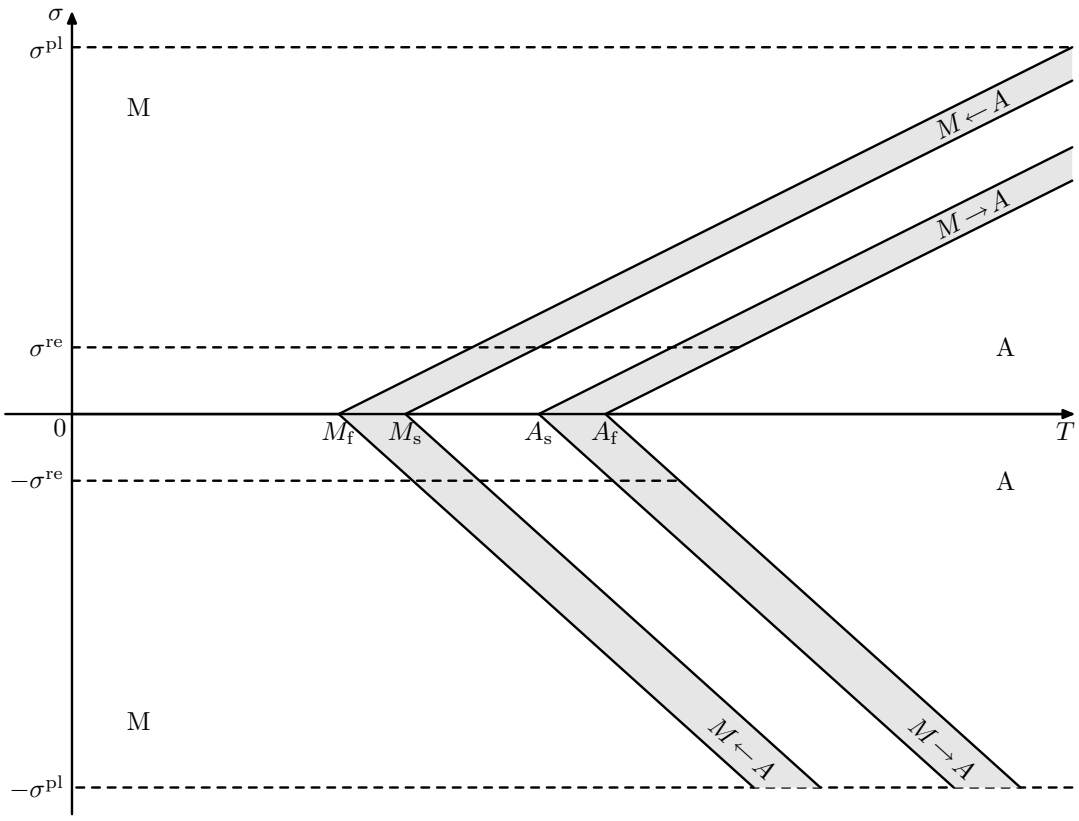

Figure 1: Stress-temperature space. Area where austenite/martensite exists denoted by 'A'/'M', transformation strips marked with grey color. See text for details.

1.2 Shape Memory Effects

For better understanding of shape memory effects, let us restrict ourselves to complex thermal and one-dimensional mechanical loading of a *single crystal* SMA specimen. This case has been very well experimentally examined and explained in many previous works (see the comprehensive paper [6] and the references cited therein, for instance) and is sufficient with respect to one-dimensional experiments performed in this work.

The activation of martensitic transformation occurs due to the presence of driving forces, either thermal or kinetic. To initiate a transformation, the chemical free energy difference between the parent and product phases must be greater than the necessary free energy barriers, such as transformational strain energy or interface energy. The space parameterized by stress, σ, and temperature, T, is commonly used, since the thermodynamic driving force depends only on stress and tempera-

[1] more often, but less precise termed *single-variant martensite* in the literature

ture in a very good approximation. The stress-temperature (σ-T) space is referred to as the phase space and it is depicted in figure 1.

In the figure, the transformation temperatures M_s, M_f, A_s and A_f indicate the start and finish temperatures at zero stress for martensite and austenite production, respectively. σ^re and $-\sigma^\mathrm{re}$ denote the critical finish stresses of martensite reorientation processes, $\sigma^\mathrm{pl}/-\sigma^\mathrm{pl}$ indicates the value of stress above/under which plastic slip occurs.

Depending upon the path taken within the phase space, certain characteristic features of the stress-strain response will manifest themselves. If austenite is cooled from above A_f to below M_f at zero stress, the resulting effect will be the creation of a self-accommodating (or twinned) microstructure. This process begins at M_s and completes at M_f. The ensuing multiple variants, which form, tend to average the overall deformation to a net zero change in shape on the macroscopic scale (neglecting thermal expansion). If this material is subsequently mechanically stressed, the multiple variants will coalesce into one variant in the preferred direction of loading, in a process of *reorientation* (also known as detwinning). This process finishes at σ^re. Upon removal of the mechanical load, a permanent deformation is retained in the specimen. (*Preferential variants* are stable until the loading direction is reversed, i.e. from tension to compression or vice versa.) This is sometimes called *pseudoplasticity* or *quasiplasticity*. If the material is now heated above the critical temperature A_f, it reverts to austenite and completely recovers its original shape – i.e. the so-called *one-way shape memory effect*. The recovery process begins at A_s and completes at A_f, see a schema of the process in the temperature-strain-stress space, figure 2.

In SMAs studies, the Clausius-Clapeyron equation is used to approximate the value of the critical stress inducing the martensitic phase transition (see author's previous work [7] for details). The Clausius-Clapeyron equation has the form

$$\frac{\mathrm{d}\sigma}{\mathrm{d}T} = \frac{\rho \Delta S}{\Lambda}, \tag{1}$$

where σ denotes (one-dimensional) stress, ρ is density of martensite (or austenite, because the difference between their densities is very small), ΔS denotes specific entropy change due to phase transition and Λ is (maximum) transformation strain. For experimental reasons, the usual form is

$$\frac{\mathrm{d}\sigma}{\mathrm{d}T} = \frac{\rho h}{T\Lambda}. \tag{2}$$

Both transformation heat, $h := T\Delta S$, and transformation strain, Λ, are well-measurable quantities. The entropy change Δs is usually considered to be *temperature independent* (at least for reasonable temperature ranges it is well-satisfied assumption) and the *critical transformation slope*

$$s := \frac{\rho \Delta S}{\Lambda} \tag{3}$$

is considered as temperature independent. Hence, the equation

$$\frac{\mathrm{d}\sigma}{\mathrm{d}T} = s \tag{4}$$

reflects the experimental observations, in which the uniaxial stress required to induce the martensitic transformation in SMA is (approximately) linearly dependent on the temperature T.

When the temperature is above the finish temperature A_f and the specimen is loaded mechanically above a critical stress level given by Clausius-Clapeyron equation the austenite starts to transform into a martensite with respect to the direction of loading, accompanied by a large macroscopic strain, so-called *transformation strain*. The critical stress level is marked as two diagonals – one for tension, one for compression – starting at M_s in figure 1. The transformation is finished by crossing the diagonals starting form M_f. The strain is recovered upon removal of the mechanical load in a reverse process, since martensite is not stable at low stress and high temperatures and it transforms into austenite in the stripe of σ-T plane bounded by parallel lines starting in A_s and A_f temperatures. Typically, this type of process is called *superelasticity* (or *pseudoelasticity*), since the behavior is similar to elasticity – the material returns to its initial configuration upon removal of the loading. Let us recall this processes are possible due to reversibility of MT, which is specific for SMAs.

In a typical loading-unloading experiment under tension and compression where the stress level is assumed to be smaller than the plastic yield stress the *tension-compression asymmetry* will demonstrate itself. When martensite plates grow, different preferential crystallographic variants are favorable for tension or compression loading and thus different internal martensitic structure is established. As a result, the transformation strain induced by phase transformation under compression is smaller and the absolute value of stress level required to start the forward phase transformation under compression is higher than that of the tension experiment. Experimentally, a wider hysteresis loop along the stress axis is observed under compression and the size of the stress-strain hysteresis along the strain axis is considerably smaller under compression. The different critical stress level for MT in tension and compression at fixed temperature (see figure 1) is due to different values of maximum transition strain Λ for tension and compression in the Clausius-Clapeyron equation.

When changing the direction of stress under M_s (tension to compression or vice versa), martensite variants tend to arrange themselves in the preferred direction of loading. This process of *reorientation* of inappropriately oriented variants also finishes at (approximately temperature-independent) values σ^re and $-\sigma^\mathrm{re}$ for tension and compression, respectively, and it is analogous to detwinning. This process contributes to change of the total strain of the specimen.

Since the response of the system depends not only on the current values of stress and temperature but also on their previous values ("direction of evolution"),

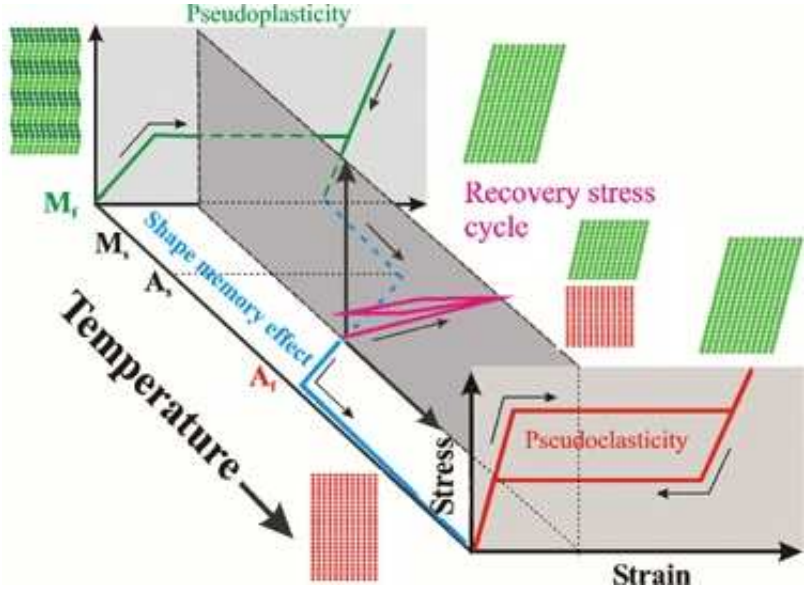

Figure 2: Stress-strain-temperature space. Some important shape memory effects are sketched. See text for details. Reprinted from [8].

hysteresis is a manifestation of "memory" in the system. An interesting property of hysteresis in SMAs is the *return point memory* (RPM), global memory of the system. After a cyclic variation of the driving, the system follows exactly the same trajectory that it would have followed if the cyclic variation had not taken place. In this way, a hierarchy of loops within loops is formed, each *internal subloop* being characterized by the point at which it was initiated – *return point* – i.e. by the point, where the direction of loading is changed. Results of RPM experiments can be summarized by the following [9].

- The path resulting from complete forward transformation and complete reverse transformation sets the boundaries of the two-phase region, where RPs may occur. The transformation path followed by the system in this two-phase region depends on its previous history through the ensemble of return points in the path.
- The influence of a return point on the evolution of a transformation path disappears when the transformation path reaches the return point again. At the same time the influence of previous return point, constituting the same internal subloop, also disappears and system evolutes as the subloop has never been formed. This phenomena is called *wiping out property*.
- The RPM in SMA is very well established in polycrystals and very often found in single crystals, in both thermally and stress-induced transformations, although differing behaviors have also been reported in the last case.

Different behavior mentioned in the last item refers to experimental results, in which the memory of the return points evolves with time. Some observations also show the hysteresis loop is sensitive to the transformation rate. Both abnormalities are related and, rigorously, they would be in contradiction with the basic physical assumption of *reversible athermal* MT. But they can be easily explained by the progressive difficulty in evacuating or absorbing the transformation latent heat at high strain rates (the latent heat not absorbed by environment increases the temperature of specimen, which changes transformation conditions) or irreversible internal evolution of microstructure SMA (e.g. ageing). If the loading is quasistatic and the ambient temperature is kept constant, the hysteresis loops tend asymptotically to be independent on the strain rate.

Since hysteresis in present even in martensite reorientation, the process of reverse transformation from tensile martensite to austenite occurs also in negative stresses between the lines starting at points $A_\mathrm{s}, A_\mathrm{f}$ prolonged from $\sigma \geq 0$ half space (and similarly for compressive martensite) (see [10]).

Partial (transformation) cycle is another often referred term connected with hysteretic behavior. By partial cycle we mean a thermomechanical cycle, at which the initial and the final state of material are the same pure phase (martensite or austenite), the phase transition is initiated but, due to one abrupt reversion of driving during the cycle, it is not completed.

Reaching the σ^{pl} stress level in tension or $-\sigma^{pl}$ stress level in compression, the processes determined by plastic deformation as plastic slip or creep occurs.

The *two-way shape memory effect* (TWSME) is usually considered as a phenomenon of spontaneous direct and backward change of the sample shape with thermal cycling in the temperature range of martensitic transformations. When an alloy is plastically deformed in martensitic state, the spontaneous reversible shape change on cooling during thermal cycling through the temperature range of the martensitic transformations occurs in the direction of the preliminary deformation of martensite and is called "positive" or "martensitic". The TWSME of the opposite sign ("negative" or "austenitic") appears after the deformation of the austenite. The TWSME value depends on internal stress fields generated by dislocation substructure, precipitated particles or having another origin. It also depends on on alloy composition or concentration of solid solution. It is believed that dislocation arrays, retained martensite and residual stress fields are necessary to obtain some TWSME. Therefore, heat and thermomechanical treatments are effective for TWSME regulation. Although this effect can be obtained by various processes such as superelastic or shape memory training, thermomechanical training, aging under external stress, etc., one of the simplest processes may be a single high deformation applied in the austenite or martensite state [11].

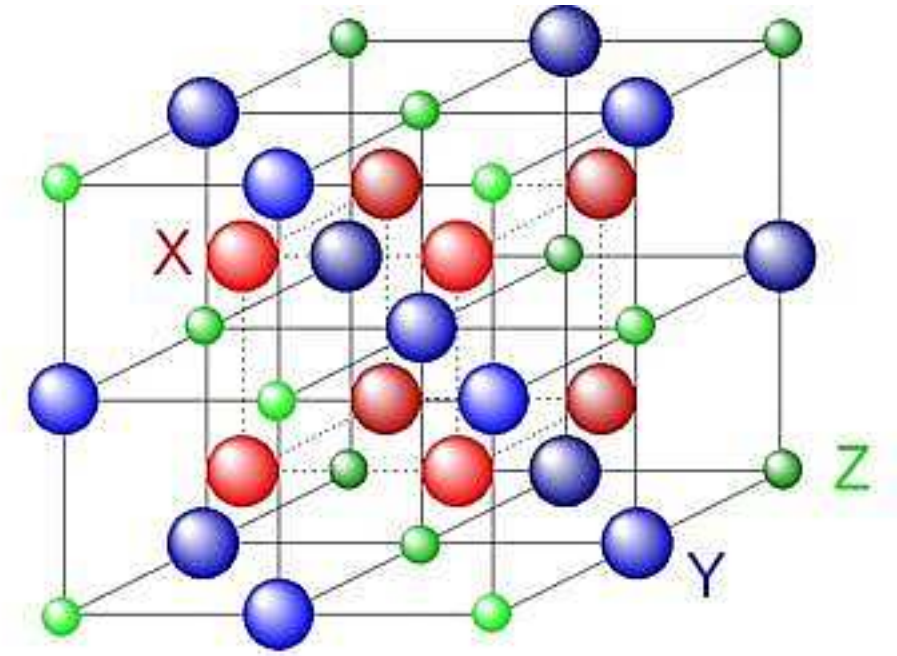

Figure 3: Crystal structure of Heusler alloys. The X position are occupied by nickel atoms, the Y positions by manganese and the Z positions by gallium atoms in the case of Ni_2MnGa stoichiometric alloy. Reprinted from [12].

1.3 Ni-Mn-Ga Based Shape Memory Alloys

Many alloys exhibiting SMEs have been discovered since 1950s. Due to type of the martensitic crystallographic lattice in a pure single crystal, we can distinguish these groups of SMAs (number of crystallographic variants and some examples are given):

- tetragonal lattice (3) – InTl, Ni_2MnGa, NiAl, FePt
- orthorhombic lattice (6) – AuCd, CuNiAl
- monoclinic lattice (12) – CuZn, CuAlZn, NiTi

Only some of these can be produced and manufactured at reasonable price and hence are useful for commercial use.

From the point of view of future applications, the most promising magnetic SMAs are nickel, manganese and gallium based alloys with composition near to the stoichiometric one. So far, the application development based on the MSMA elements has mainly concentrated in actuators, such as proportional fluid valves, linear motors and optical applications, but thin-films and composites introduce totally new possibilities and an exceptional multifunctionality can be obtained when the alloy is utilized for actuating, sensing and energy harvesting. A review of specific properties of Ni-Mn-Ga based SMAs with respect to possible applications can be found in [13].

For the stoichiometric composition Ni_2MnGa the martensitic transition temperatures are $M_s = 207\,\mathrm{K}$, $M_f = 193\,\mathrm{K}$, $A_s = 209\,\mathrm{K}$, $A_f = 221\,\mathrm{K}$. However, these

temperatures are heavily dependent on the chemical composition and it is possible to increase the transition temperatures to be close to room temperature [14] by composition changes. The Curie temperature, T_C, connected to the temperature region of magnetic transition from paramagnetic to ferromagnetic is 376 K and slightly fluctuates around this value under a wide composition range [15, 16].

The parent β phase (austenite) is a cubic $L2_1$ structure (Heusler structure) in the near-stoichiometric Ni-Mn-Ga alloys (see figure 3). Several studies have been performed to examine crystallographic structure of the martensitic phase with respect to possible modulation of atom planes (e.g. [5, 17]). In addition to non-modulated tetragonal phase (NM), there are two more types of martensite usually distinguished – five-layered structure (5M) and seven-layered structure (7M).

Intermartensitic transitions are transitions, where one type transforms to another. In [18] the intermartensitic transitions were studied by different experimental techniques. Occurrence of these transitions and their transformation temperatures are strongly influenced by internal stresses and inhomogeneities or by composition. Various experimental techniques differed in sensitivity.

Magnetic field induced strain in a Ni_2MnGa single crystal was examined by Ullako *et al.* for the first time (see [19]). It is only observed in layered martensite: about 6 % MFIS is obtained in the five-layered structure and 10 % in the seven-layered one. The easy magnetization axis always coincides with the shortest crystallographic axis of the modulated martensite while applying the coordinate system of the cubic phase. The coupling of the crystal structure and the magnetic domain structure is a prerequisite for MFIS.

However, the preparation of single crystals is a time- and cost-consuming process, and there can be compositional changes along the axis of the crystal and segregations. That is why, from a technological point of view, polycrystals are of great interest. They can be easily produced, but, unfortunately, they usually exhibit lower strains because of the different orientations of the separate crystals and the presence of grain boundaries, which act as pinning centers and impede the twin boundary motion.

A possible approach to improve the polycrystalline material is to have a coarse-grained and highly textured sample, because then its properties resemble the properties of a single crystal.

During the solidification of metallic alloys, crystallized grains form structures, which may differ in different parts of the parent ingot. The structural characteristics of each part depends, among other factors, on the composition and thermophysical properties of the alloy, casting and solidification conditions (thermal gradients, kinetics) and the presence of grain refining particles. A transition from an outward, highly directional columnar grain structure to an inner equiaxed grain structure with randomly oriented grains is often observed. Grains of the columnar structure have usually preferential crystallographic orientation, thus the columnar structure

has so-called *texture*. Physical properties of columnar and equiaxed structure of Ni-Mn-Ga based alloys are different, see [20].

A successful attempt to achieve texture in polycrystalline Ni–Mn–Ga by slow directional solidification was made by Pötschke *et al.* in [21]. The stationary casting was employed to achieve coarse-grained, textured samples. The deviation of the orientation of the grains was small.

Except to the directional solidification texturing of material can be obtained by large plastic deformation, but high degree of brittleness of Ni-Mn-Ga alloys should be concerned [22, 23].

1.4 Deformation

In the case of uniaxial loading of an oblong specimen we can define engineering stress as ratio between force F acting on the end-side and its area S_0:

$$\sigma = \frac{F}{S_0}\,. \tag{5}$$

For description of length changes of solid material sample (induced by stress or temperature changes), the *engineering strain*, ε, is often used:

$$\varepsilon = \frac{l - l_0}{l_0}\,. \tag{6}$$

l_0 denotes the original length of the specimen and l is its actual length (after mechanical or thermal load). The same relation for a length change due to a temperature change defines the *relative elongation* (RE) of the sample.

The true strain, $\varepsilon_{\mathrm{tr}}$, is defined:

$$\varepsilon_{\mathrm{tr}} = \ln \frac{l}{l_0}\,. \tag{7}$$

The following relation is clear

$$\varepsilon_{\mathrm{tr}} = \ln \frac{l_0 + l - l_0}{l_0} = \ln(1 + \varepsilon)\,. \tag{8}$$

Therefore, it holds

$$\varepsilon \ll 1 \quad \Rightarrow \quad \varepsilon_{\mathrm{tr}} \doteq \varepsilon\,. \tag{9}$$

1.5 Dilatometry

Thermal dilatometric analysis (dilatometry) evaluates the actual length of a specimen subjected to a thermal loading. Thus, it is a useful method for research on physical or chemical processes, where volume or length changes of solid material specimen are induced by temperature change.

The change in volume of a sample V with temperature T can be described by the *coefficient of volumetric thermal expansion* $\beta(T)$ defined as

$$\beta(T) = \frac{1}{V}\frac{\partial V}{\partial T}\,. \tag{10}$$

Similarly, in each direction of the sample the *coefficient of linear thermal expansion* $\alpha(T)$ can be introduced:

$$\alpha(T) = \frac{1}{l}\frac{\partial l}{\partial T}\,, \tag{11}$$

where l denotes the length of the sample in chosen direction at temperature T. If l_i denotes length of the sample at temperature T_i, then the *mean coefficient of thermal expansion* in the temperature range (T_1, T_2) is defined as

$$\overline{\alpha}(T_1, T_2) = \frac{1}{l_1}\frac{l_2 - l_1}{T_2 - T_1} \tag{12}$$

and it holds

$$\lim_{T_2 \to T_1} \overline{\alpha}(T_1, T_2) = \alpha(T_1). \tag{13}$$

If temperatures T_1, T_2 are close enough in each measurement step and the linear coefficient of thermal expansion does not change abruptly, then $\overline{\alpha_{\mathrm{E}}}(T_1, T_2) \doteq \alpha(T_1)$ due to 13 and we can use interpolation to find function $CTE(T) \sim \alpha(T)$. This interpolated function is shortly called "coefficient of thermal expansion" and denoted CTE in this thesis.

Dilatometry is a method sensitive to any length change related to a change of temperature of the measured sample. The basic contribution to relative elongation of the sample are thermal vibrations of atoms (phonons). This contributions is manifested by a continuous change of the RE of the sample and by a slight increase of the CTE with increasing temperature.

On the other side, any discontinuous change in length of the sample at constant temperature and pressure (due to a first-order phase transition, for instance) leads to a step-like change of the RE. In the temperature dependence of the CTE the Dirac delta function would occur as a result. However, the phase transition usually extends over an appreciable temperature range, thus, a peak of finite height is measured. If the material transforms at generally higher temperatures during heating than during cooling, a hysteretic loop in the temperature dependence of relative elongation occurs.

1.6 Thermal Diffusivity and Thermal Conductivity

In the case of heat propagation in an isotropic and homogeneous medium in the three-dimensional space a transient heat transfer process is described by the heat

equation (T denotes temperature)

$$\frac{\partial T}{\partial t} = \kappa(T)\left(\frac{\partial T^2}{\partial^2 x} + \frac{\partial T^2}{\partial^2 y} + \frac{\partial T^2}{\partial^2 z}\right). \tag{14}$$

The measurable $\kappa(T)$ is called *thermal diffusivity* and it is connected to the thermal conductivity λ. The relationship between them is given by the equation

$$\kappa(T) = \frac{\lambda(T)}{\varrho(T)C_p(T)}, \tag{15}$$

where C_p is the mass-specific heat capacity at constant pressure and ϱ is the density, both temperature-dependent. The specific heat and the density are relatively structurally insensitive.

The *flash method* of determining of thermal diffusivity was first described by Parker *et al.* in 1961 in [24]. A high intensity short-duration light pulse is absorbed in the front surface of a thermally insulated specimen and the resulting temperature history of the rear surface is measured. The thermal diffusivity is determined by the shape of the temperature versus time curve at the rear surface.

If a pulse of radiant energy with area-specific density Q is instantaneously and uniformly absorbed in enough small depth at the front surface ($x = 0$) of a thermally insulated solid of uniform thickness, the time dependence of temperature $T(x,t)$ at the rear surface of the sample ($x = d$) could be expressed by

$$T(d,t) = T_{\text{amb}} + \frac{Q}{d\varrho C_p}\left[1 + 2\sum_{n=1}^{\infty}(-1)^n \exp\left(\frac{-n^2\pi^2}{d^2}\kappa t\right)\right], \tag{16}$$

where T_{amb} is the ambient temperature (see [24] for details). Due to convergence of the expression in square brackets the maximum rear surface temperature rise ΔT_{M} can be established by

$$\Delta T_{\text{M}} = \lim_{t\to\infty} T(d,t) = \frac{Q}{d\varrho C_p}. \tag{17}$$

At time t_{h} the temperature at the rear side of the sample reaches half of its maximum value and thus we get

$$T(d,t_{\text{h}}) = T_{\text{amb}} + \frac{1}{2}\Delta T_{\text{M}} \quad \Rightarrow \quad \frac{1}{2} = 1 + 2\sum_{n=1}^{\infty}(-1)^n \exp\left(\frac{-n^2\pi^2}{d^2}\kappa t_{\text{h}}\right) \quad \Rightarrow$$

$$\kappa = \frac{1.38\, d^2}{\pi^2 t_{\text{h}}}. \tag{18}$$

Since the temperature in the sample slightly varies during the process, an estimate for the *effective value* T_{ef} is needed. The result of a simple approximation suggested and determined in [24] is:

$$T_{\text{ef}} \doteq T_{\text{amb}} + 1.6\,\Delta T_{\text{M}}. \tag{19}$$

Equation (15) implies the product of the density and the heat capacity of an alloy is needed for computing thermal conductivity. Recalling (17) we get

$$\varrho C_p = \frac{Q}{d\Delta T_{\mathrm{M}}}. \tag{20}$$

Variables d and ΔT_{M} are easy to measure and Q is a parameter of the experimental apparatus constant within the temperature range for a given distance between the sample and the pulse generator. Thus, if we determine the value of Q, we can compute the product ϱC_p at any arbitrary temperature using (20) and

$$\lambda(T) = \frac{Q}{d}\frac{\kappa(T)}{\Delta T_M(T)}. \tag{21}$$

To find the temperature-independent coefficient Q/d it is enough to know density, heat capacity and the maximum rear surface temperature rise ΔT_{M} at one reference temperature.

For evaluating the heat capacity the *Neumann-Kopp rule* can be used. It can be formulated as:

> The heat capacity of 1 mole of a solid substance is approximately equal to the sum over the elements forming the substance of the heat capacity of a gram atom of the element times the number of atoms of the element in a molecule of the substance.

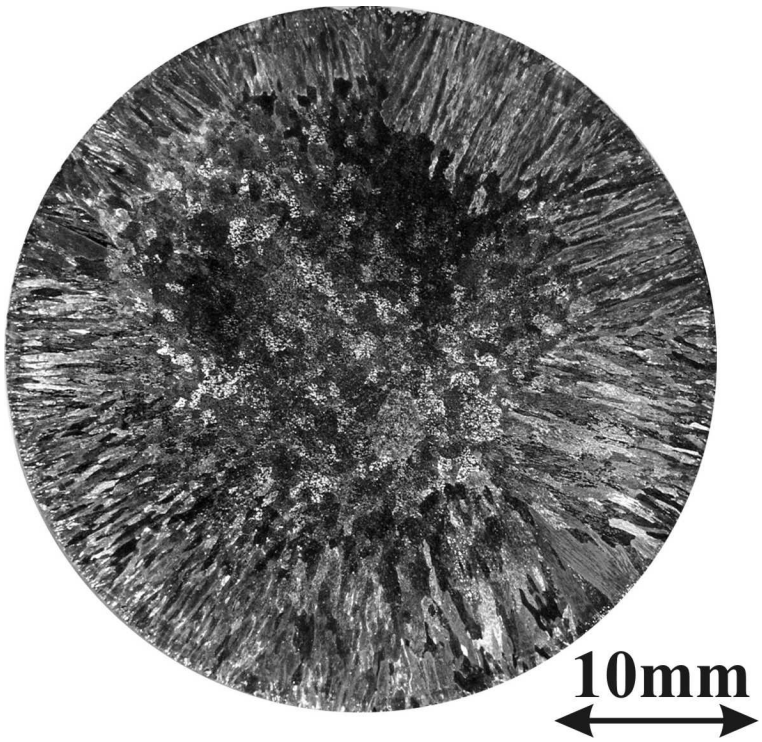

Figure 4: Structure of ingot in the cross-section. Courtesy of A. Jäger.

2 Experimental

2.1 Materials

A polycrystalline ingot of $Ni_{53.6}Mn_{27.1}Ga_{19.3}$ alloy (diameter 40 mm, length 100 mm) was prepared by arc melting of the elements under argon atmosphere at reduced pressure at the Institute of Physics, Academy of Sciences of the Czech Republic. It was thermally stabilized for one hour. Casting temperature was about 1700 K. The microstructure in cross-section is shown in fig. 4. The microstructure reveals three distinct regions. The central zone and the chill zone of the ingot are composed of equiaxed grains (see figure 5) and the rest of the ingot consists of columnar grains, which grew from nuclei localized at mould walls into the melting (fig. 6). The samples were prepared by electrical discharge machining and grinding from the part of the ingot with columnar structure. The longitudinal direction of columnar grains is perpendicular to the axis of the samples. The samples were annealed for 4 days at 1100 K. Composition of the samples was determined with AAS Perkin Elmer spectrometer and ICP Spectro spectrometer at VÚT Panenské Břežany.

The dimensions of the samples were (6.0 ± 0.1) mm in diameter and (24.93 ± 0.01) mm in length in the case of cylindrical samples for dilatometric measurement and (1.56 ± 0.02) mm in length and (16 ± 1) mm in diameter in the case of disk-shaped samples for the thermal diffusivity measurements.

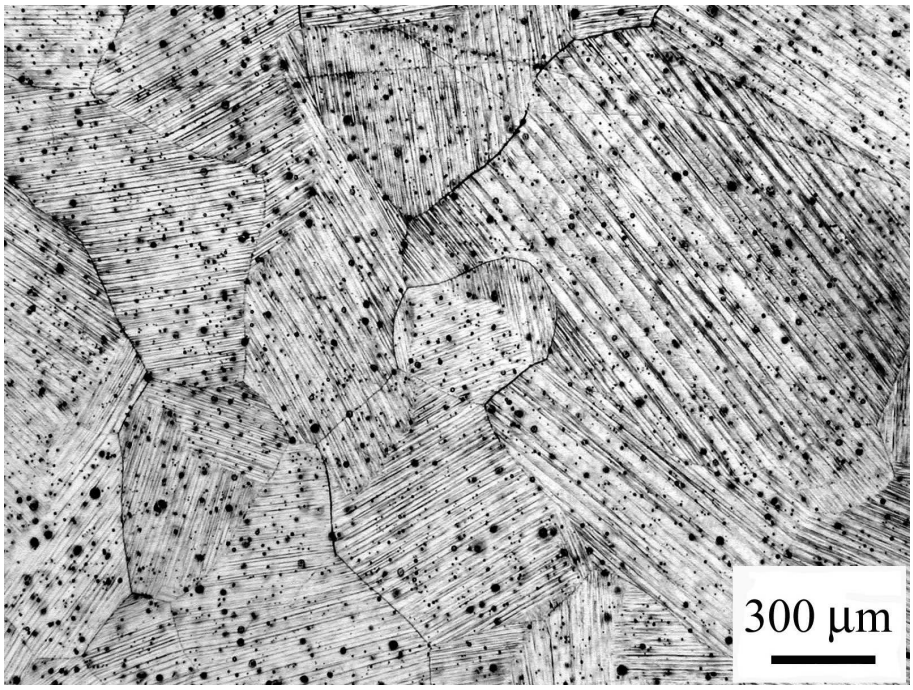

Figure 5: Microstructure of the equiaxed structure. Courtesy of A. Jäger.

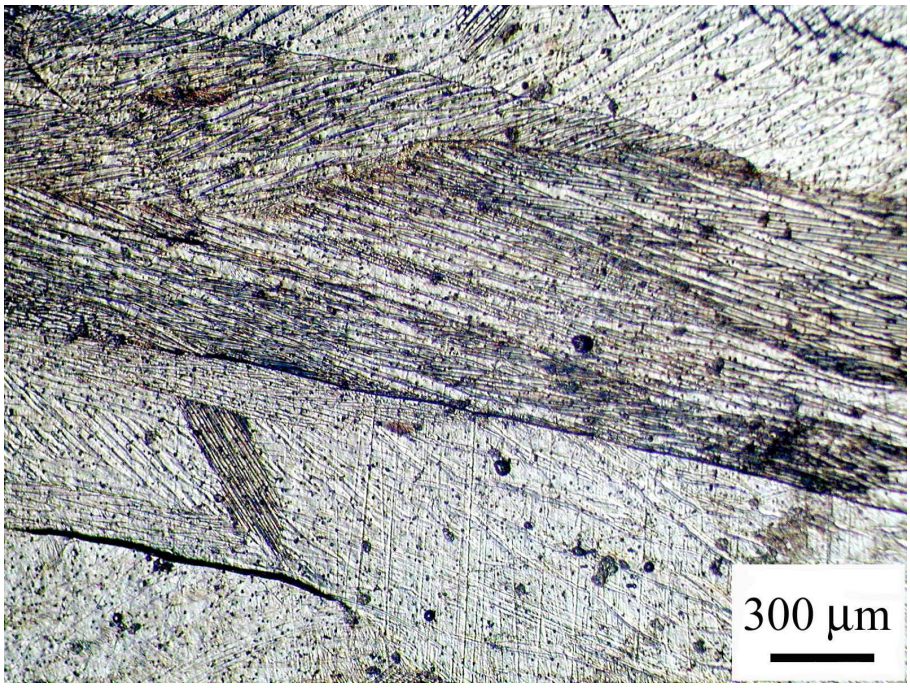

Figure 6: Microstructure of the columnar structure. Courtesy of A. Jäger.

2.2 Dilatometric and Deformation Measurements

Linear thermal expansion of the sample was measured under helium atmosphere using Netzsch 402 C dilatometer in the temperature range of 300–650 K. In all cases the thermal cycle started at room temperature, which is below both martensitic and magnetic transition temperatures. The sample was continuously heated to the maximum temperature 650 K and then the temperature was decreased. The heating rate and the cooling rate were the same for the particular cycle. The accuracy of the measuring apparatus was checked by determining the coefficient of thermal expansion for pure magnesium and comparing it with data available in the literature. The agreement between measured values and values in the literature was better than 3% difference.

In the first series of measurements the influence of heating/cooling rate to dilatation characteristics of undeformed sample was studied. Two thermal cycles were performed for each of heating/cooling rates $0.5\,\mathrm{K\,min^{-1}}$, $2\,\mathrm{K\,min^{-1}}$ and $5\,\mathrm{K\,min^{-1}}$.

The dilatation characteristics of pre-deformed alloy were studied next. The sample was deformed in compression in four steps up to -3.8% final deformation at room temperature. Deformation was performed at Instron-1186-type deformation machine and the cross-head displacement speed was $0.1\,\mathrm{mm\,s^{-1}}$. After each deformation step dilatation characteristics in two thermal cycles were determined; these thermal cycles were the same as for undeformed samples . In the fifth deformation step a macroscopic rupture occurred in the sample.

2.3 Thermal Diffusivity Measurements

The coefficient of thermal diffusivity was measured in the temperature range from 300 to 650 K by the flash method with an apparatus described in [25, 26]. The sample was placed in the center of a furnace filled with argon atmosphere. The front face of the sample coated with soot was irradiated by a short pulse of radiant energy (homogenized by optical light conductor) from a xenon pulse generator (irradiation time was of about 1 ms, wavelengths up to $1\,\mu$m). The measurements were performed at several distances between the pulse generator and the sample so that the influence of heating energy on the temperature rise in the transient temperature range could be studied. The resulting temperature rise of the rear surface of the sample was measured with a chromel/alumel thermocouple and displayed on an oscilloscope screen. Thermal diffusivity values were automatically computed from the temperature rise versus time data using equation (18).

The thermal diffusivity of an Armco iron sample was measured to check the accuracy of the apparatus (Armco iron is a standard material for the thermal diffusivity and thermal conductivity measurements). The difference between measured values and values in the literature was less than 3%.

3 Results

3.1 Dilatometry – Undeformed Sample

The thermal expansion of the undeformed sample was measured at three heating/cooling rates. The influence of the heating/cooling rate on the temperature induced relative elongation was examined. The results are summarized in figures 7, 8 and 9.

The martensitic phase transformation is induced by temperature in the sample. In figure 7 a detail of the temperature dependence of strain for is shown. An abrupt increase/decrease in the RE during heating/cooling is due to proceeding martensitic transformation. These abrupt changes occurred in the temperature range 430–470 K. As can be seen, with increasing heating/cooling rate the hysteretic loop related to the MT becomes wider (up to 6 K difference between 0.5 K min^{-1} and 5 K min^{-1}). The MT also demonstrates itself as the main peak in cooling and heating branch of the temperature dependence of the CTE in figure 8. The main peak becomes lower and shuffle with increasing heating/cooling rate, see table 1. However, the whole area under the peaks is approximately independent on the heating rate.

A detailed picture of temperature dependence of the CTE in the temperature

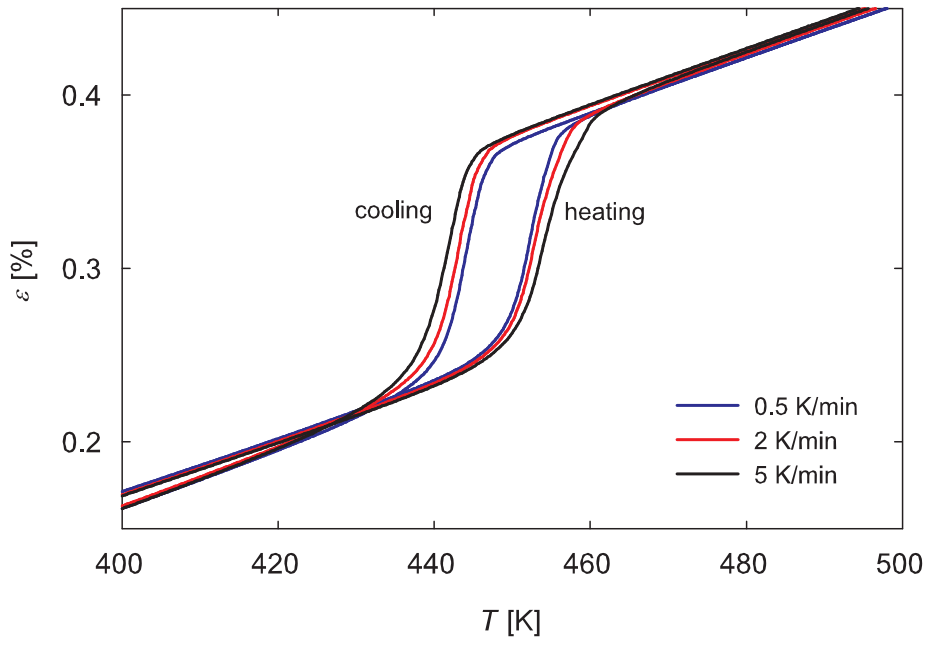

Figure 7: Temperature dependence of RE for the second thermal cycles at given heating/cooling rates in detail.

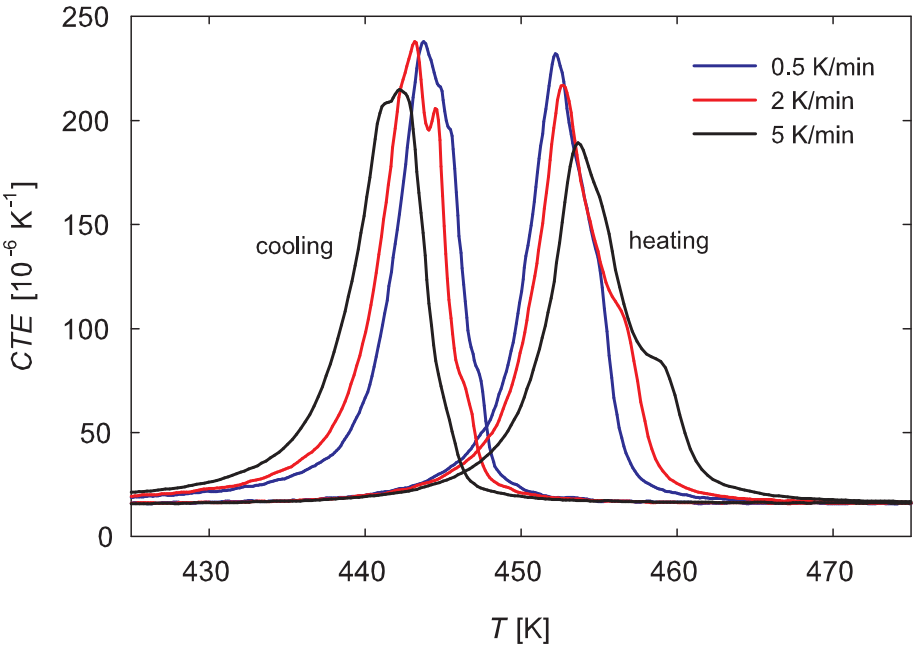

Figure 8: Temperature dependence of CTE for the second thermal cycles at given heating/cooling rates in detail.

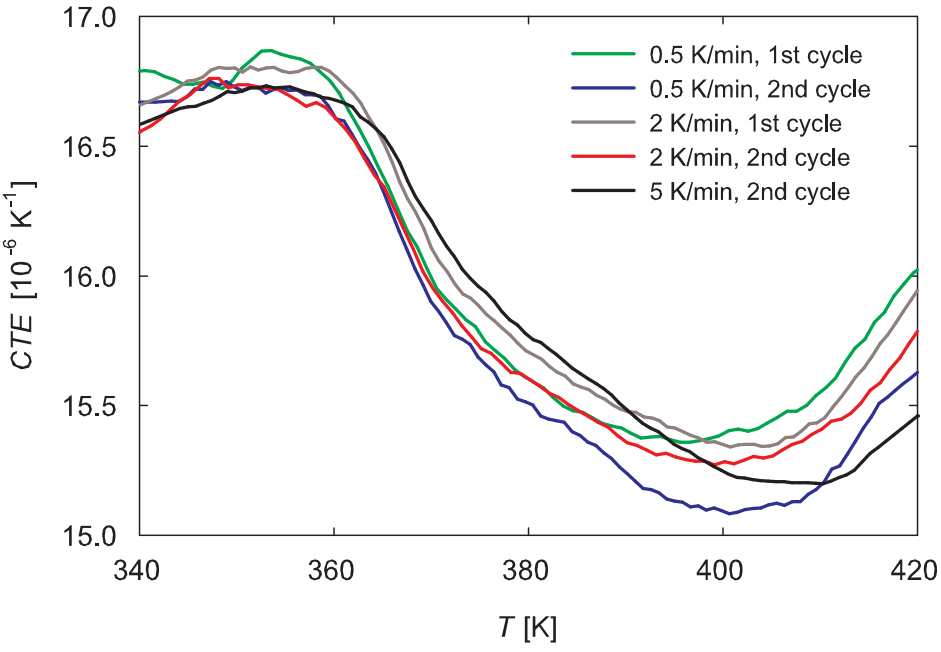

Figure 9: Anomalous decrease of temperature dependence of CTE for five heating branches at various heating rates.

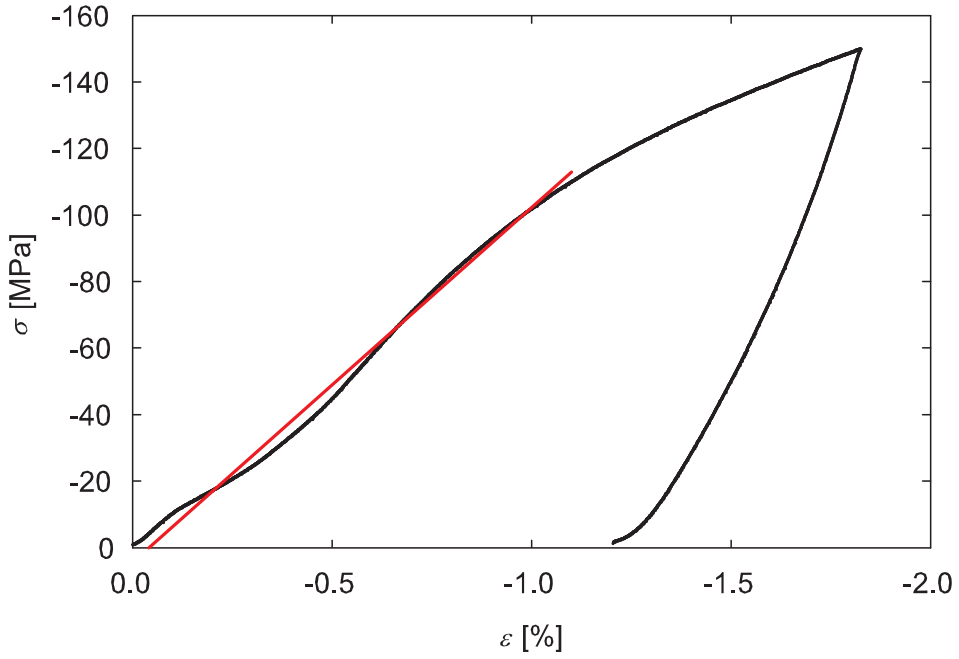

Figure 10: Stress-strain dependence at the first pre-deformation step. Elastic part denoted by a red line.

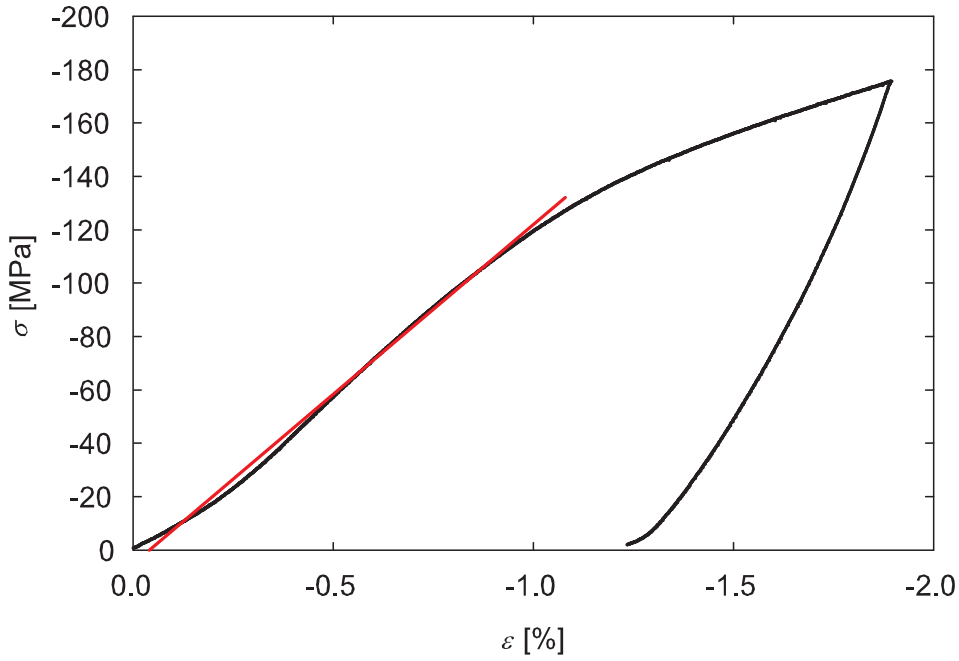

Figure 11: Stress-strain dependence at the second pre-deformation step. Elastic part denoted by a red line.

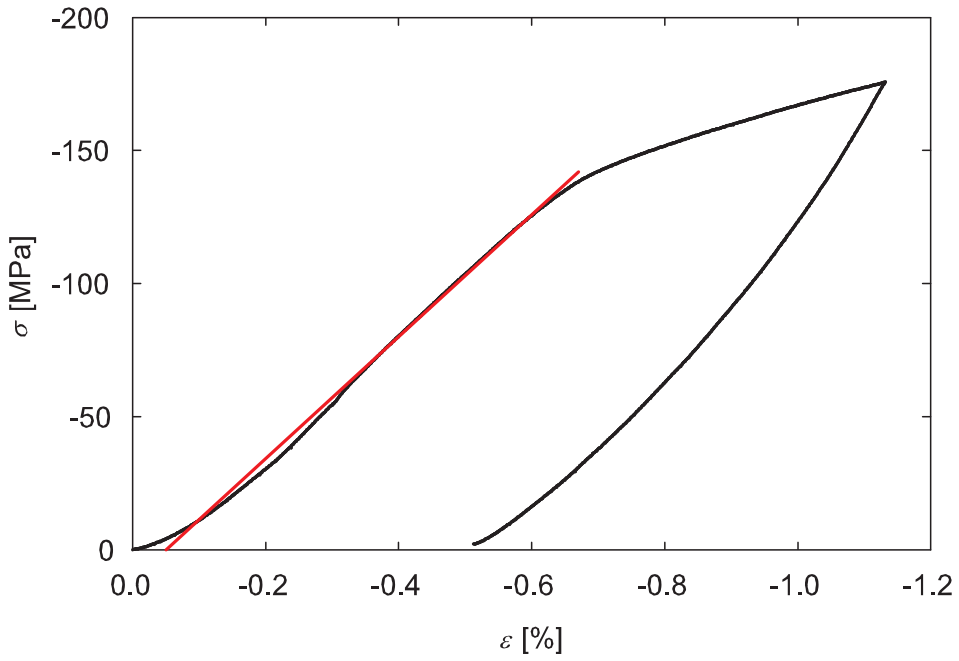

Figure 12: Stress-strain dependence at the third pre-deformation step. Elastic part denoted by a red line.

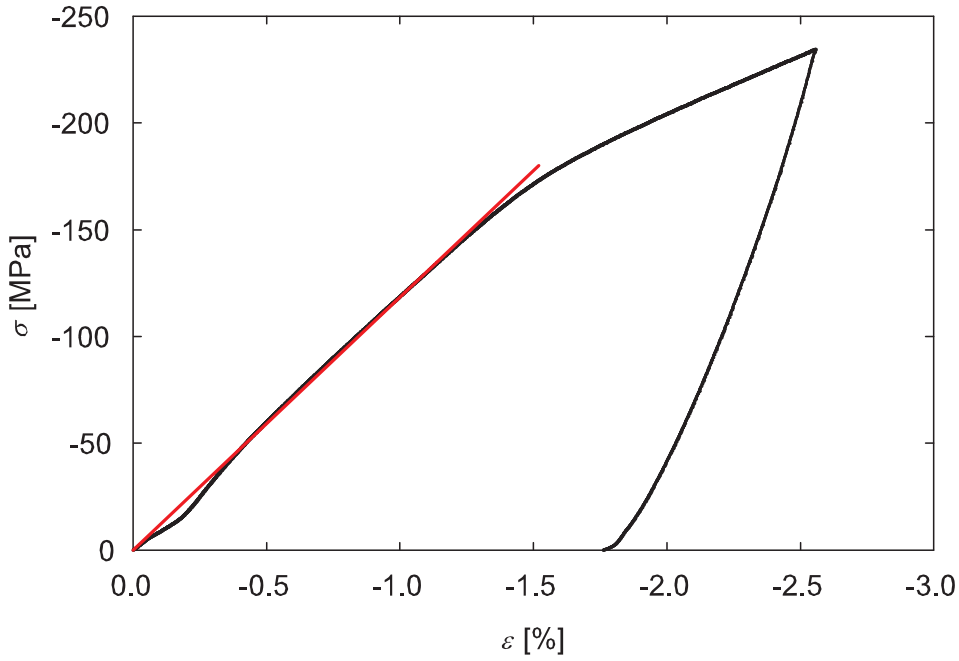

Figure 13: Stress-strain dependence at the fourth pre-deformation step. Elastic part denoted by a red line.

heating/cooling rate [Kmin^{-1}]	T_h [K]	T_c [K]
0.5	452	444
2	454	443
5	454	442

Table 1: Influence of heating/coolin rate to the temperature of the main peak of the MT. Temperature of the maximum of the peak of CTE in the heating branch is denoted by T_h, the same temperature in the cooling branch is denoted by T_c.

range 340–420 K for several thermal cycles is in figure 9. A substantial decrease of the CTE above 360 K should be noticed.

3.2 Deformation

Figures 10–13 depict the stress-strain curves for four pre-deformation steps. The values of strain are negative, since the deformation is in compression. The negative values of stress are due to convention introduced in chapter 1 (stress in tension – positive values, stress in compression – negative values). In each figure the elastic part of deformation curve is denoted by red line. The transition between the elastic part and the pseudoplastic part occurs at the critical reorientation stress σ_c. The value of this critical stress (obtained as the final point of red-marked elastic part) and the maximum value of deformation stress and strain for each step can be found in table 2. (The values of the maximum deformation strain are related to the length of the sample *before deformation*).

3.3 Dilatometry – Pre-Deformed Sample

Before the first deformation and after each deformation step the dilatation characteristics of the sample were measured. They are called "thermal cycles after (pre-) deformation" and denoted TCAD below. The temperature dependence of relative elongation for the first and the seconds thermal cycles after pre-deformation

pre-deformation step	σ_c [MPa]	σ_max [MPa]	ε_max [%]
1	−110	−150	−1.9
2	−130	−176	−2.6
3	−140	−176	−2.1
4	−180	−235	−3.8

Table 2: Critical stress, σ_c, maximum deformation stress, σ_max, and maximum deformation strain, ε_max, at four pre-deformation steps. (Values of critical stress rounded to tens.)

are in figure 14 and 15, respectively. The compression deformation releases mostly during heating in the first thermal cycles after pre-deformation, *i.e.* the thermal cycles terminate at positive values. In the second runs the recovered strain is less than 0.1%. The width of the hysteretic loops in the second thermal cycles slightly increases.

For a better understanding of the processes occurring in the studied alloy, it is useful to divide the measured relative elongation into several additive contributions. (Their meaning is discussed in the next chapter.) By subtracting the relative elongation obtained in the second TCAD from that obtained in the first TCAD, we obtain the temperature dependence of the relaxed strain, which is connected with one-way shape memory effect. In this work it is termed "residual strain" and is denoted by black lines in figures 16–19. A "tooth" in the heating branch is well perceptible in all figures.

The temperature dependence of the deformation that was obtained as the difference between the relative elongation of the second thermal cycle of the pre-deformed sample and the one before pre-deformation is denoted by red lines in figures 16–19. The changes of this strain are reversible with respect to temperature and this deformation is termed "stored strain" thereinafter. After the third and the fourth deformation small peaks occur both at heating and cooling branches.

Figure 20 and 21 summarize development of macroscopic strain in the sample for all pre-deformation steps and subsequent thermal cycles. At the beginning – experimental step 0 – the sample is undeformed. Four pre-deformations – experimental steps 1, 4, 7, 10 – were followed by the first TCAD – experimental steps 2, 5, 6, 11 – and by the second TCAD – experimental steps 3, 6, 9, 12.

In figure 20 the final strain after unloading, $\varepsilon_{\mathrm{def}}$, in a single deformation step is denoted by a blue triangle. The relative elongation after the first/second thermal cycle after deformation, $\varepsilon_1/\varepsilon_2$, is denoted by a black/grey circle. The maximum absolute deformation in a deformation step, $\varepsilon_{\mathrm{max}}$, is denoted by a green triangle in this figure as well as in figure 21.

The residual strain, $\varepsilon_{\mathrm{res}}$, is denoted by a black triangle and the critical reorientation stress, σ_{c}, is denoted by a pink triangle in figure 21. A relative elongation, which releases during the phase transformation from martensite to austenite (sample length increases steplike) and occurs once more during the reverse phase transformation (the steplike decrease of sample length), was determined from fig. 15 for each deformation step. This reversible elongation is related to the one-way shape memory effect, thus it is denoted $\varepsilon_{\mathrm{TW}}$ in figure 21.

Figure 22 reveals the temperature dependence of the CTE for the first TCAD and figure 23 reveals the same dependence for the second TCAD. They can be easily compared. Generally, the heating peaks are higher and wider than the corresponding cooling peaks. The linear coefficient of thermal expansion slightly increases in the temperature ranges 300–350 K and 550–650 K.

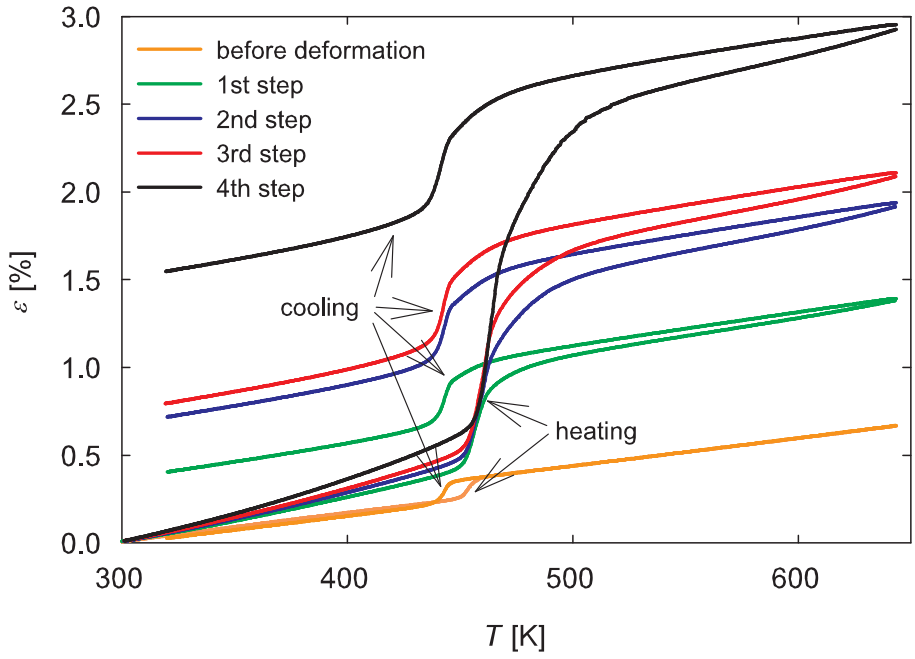

Figure 14: Temperature dependence of RE for the first thermal cycles after pre-deformation.

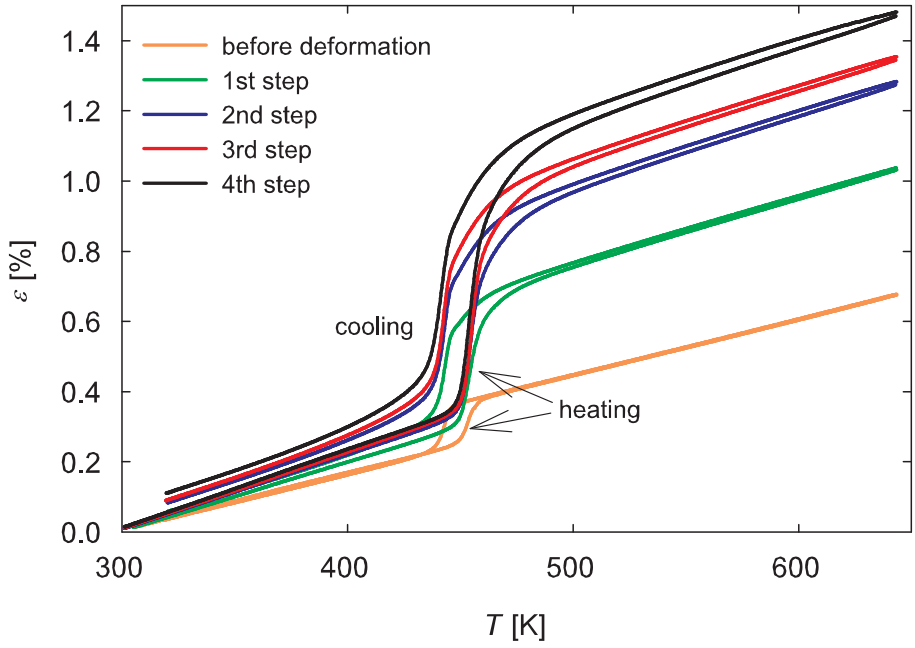

Figure 15: Temperature dependence of RE for the second thermal cycles after pre-deformation.

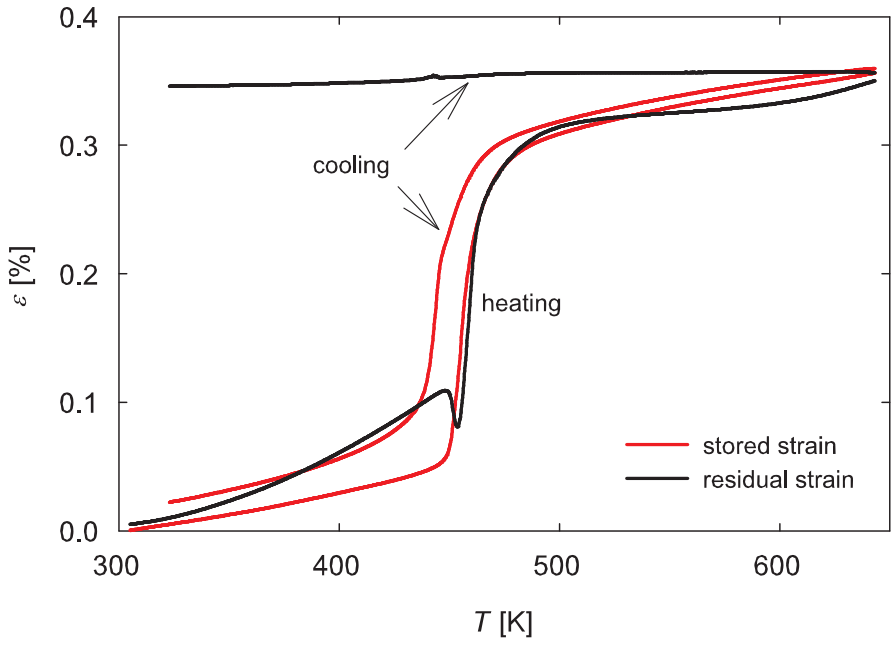

Figure 16: Temperature dependence of residual and stored strain after the first pre-deformation. See text for details.

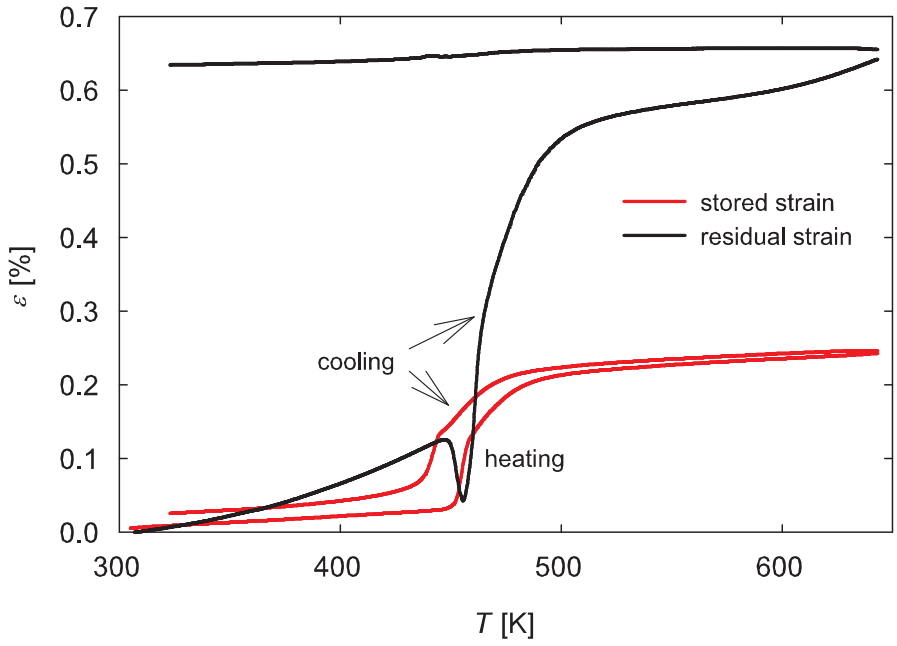

Figure 17: Temperature dependence of residual and stored strain after the second pre-deformation. See text for details.

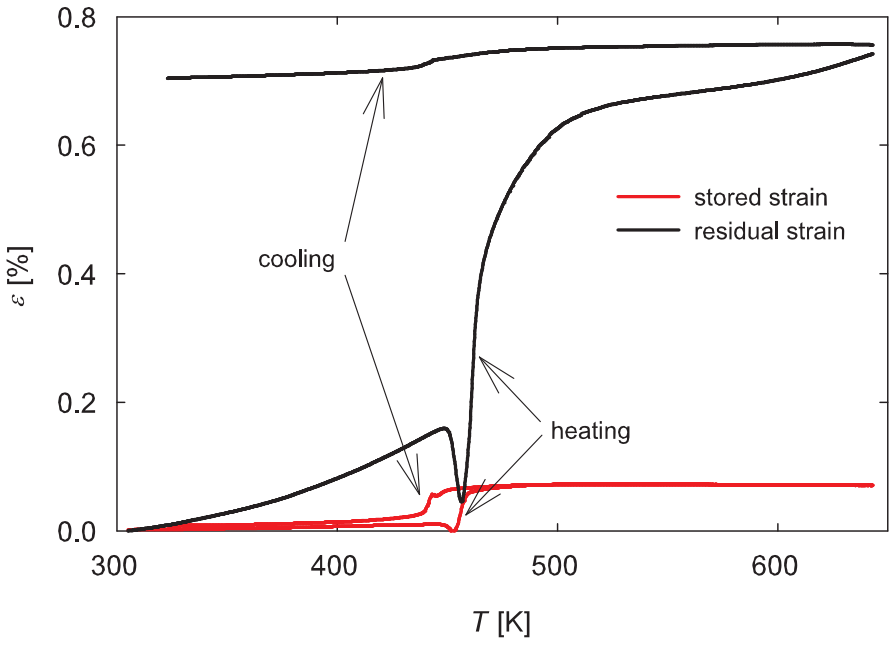

Figure 18: Temperature dependence of residual and stored strain after the third pre-deformation. See text for details.

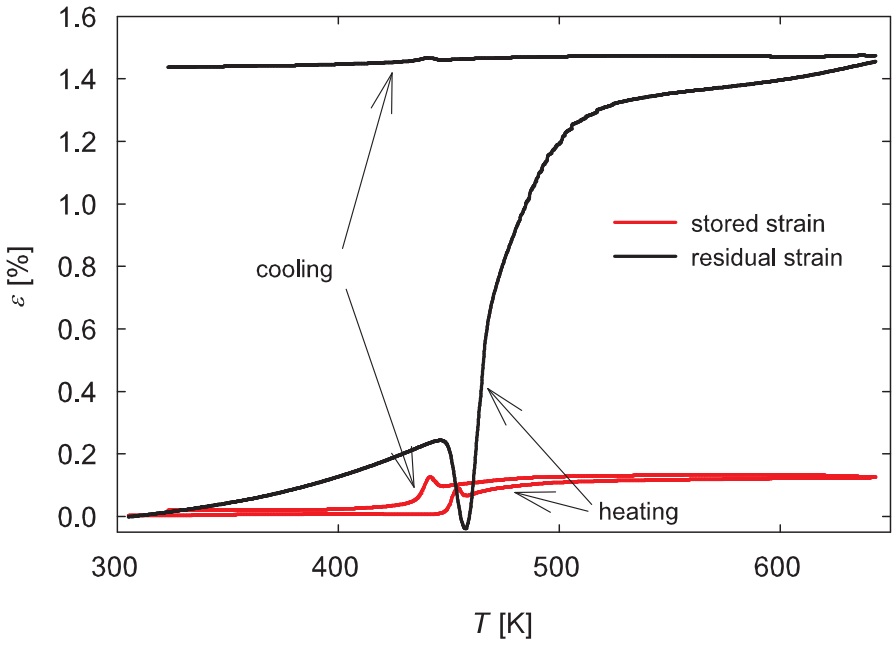

Figure 19: Temperature dependence of residual and stored strain after the forth pre-deformation. See text for details.

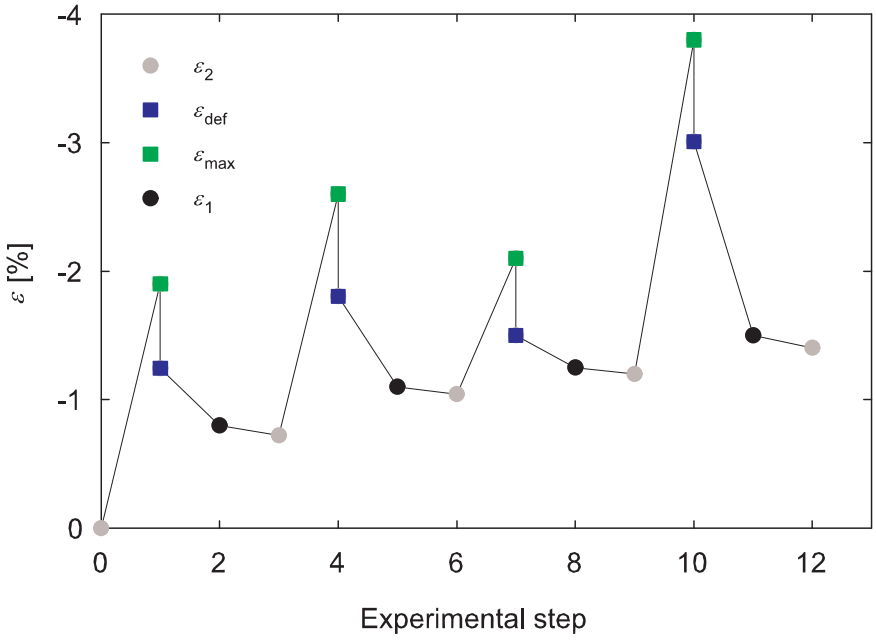

Figure 20: Evolution of the strain of the sample. See text for details.

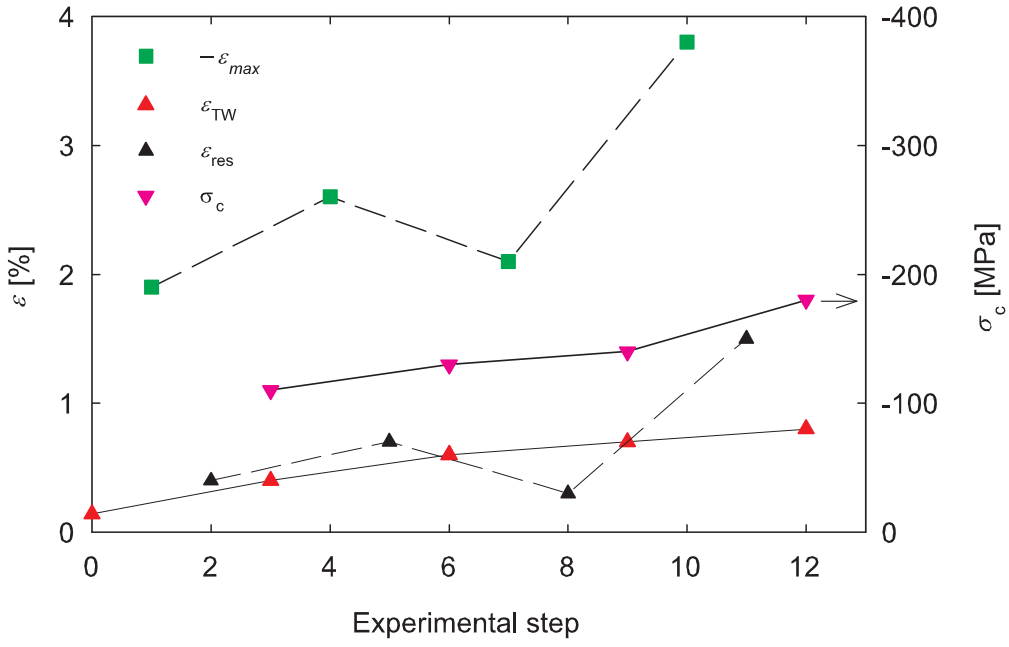

Figure 21: Evolution of some important parameters of the sample. See text for details.

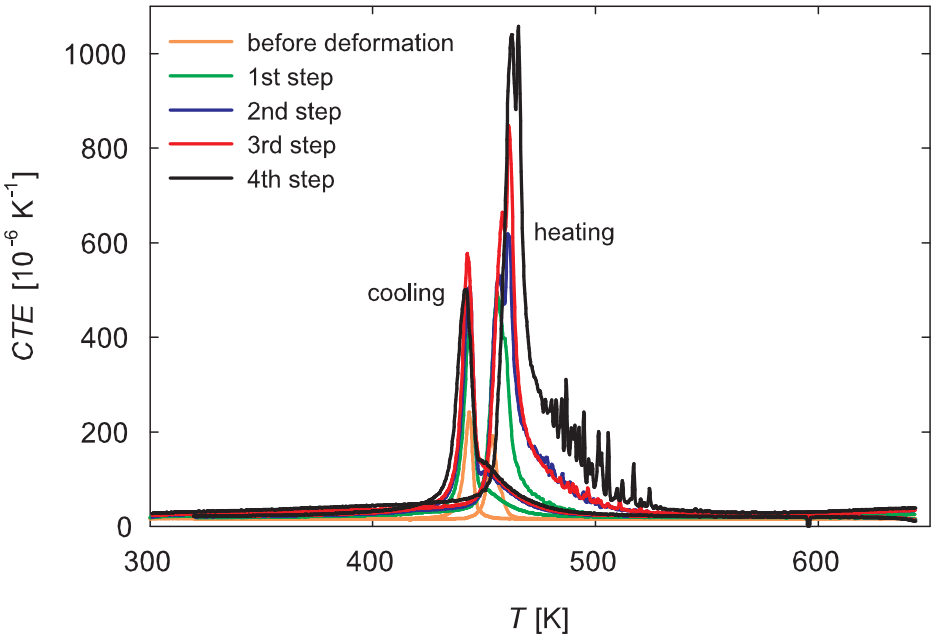

Figure 22: Temperature dependence of CTE for the first thermal cycles after pre-deformation.

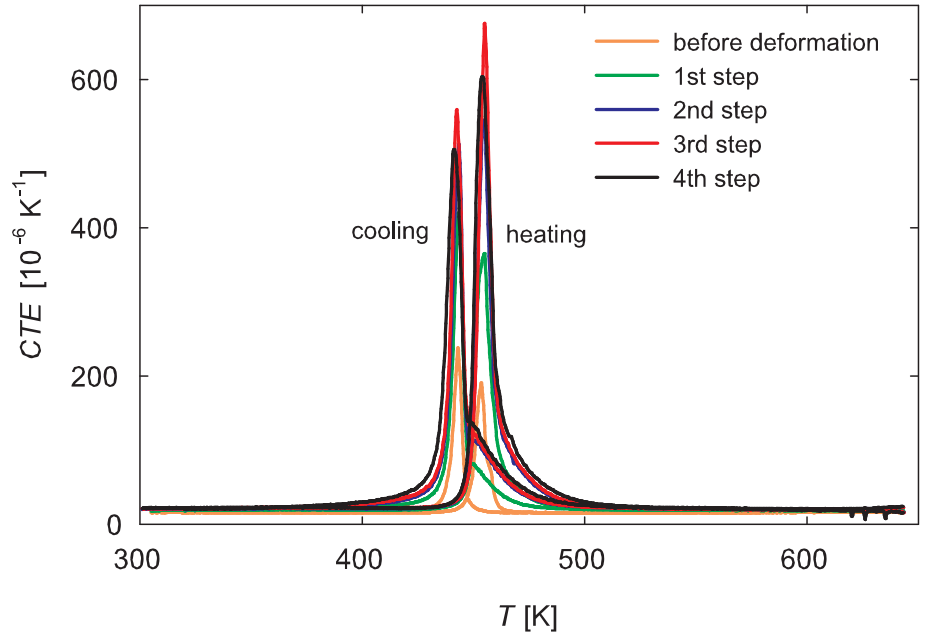

Figure 23: Temperature dependence of CTE for the second thermal cycles after pre-deformation.

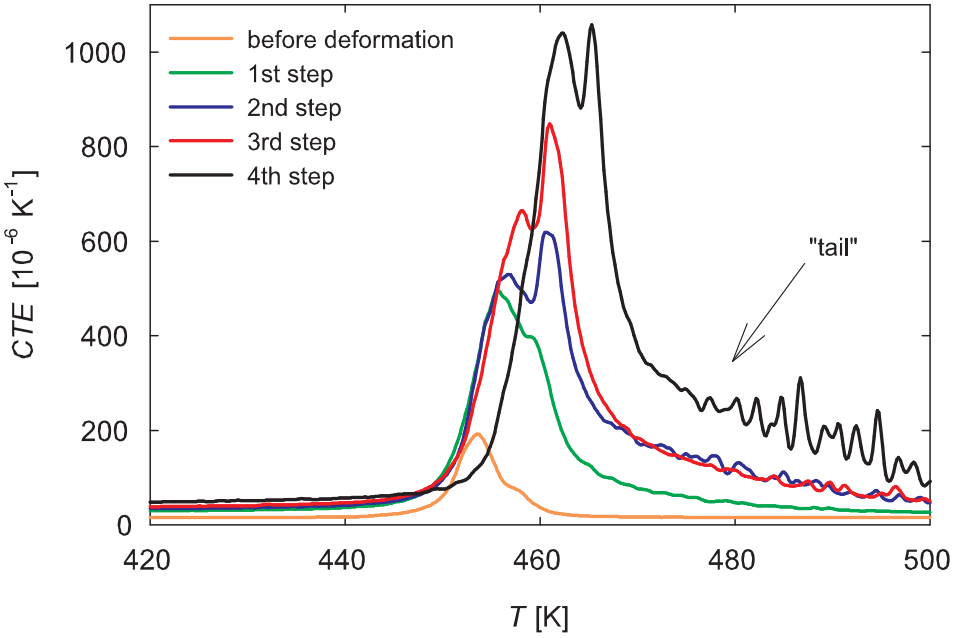

Figure 24: Temperature dependence of CTE for the heating branch of the first thermal cycles after pre-deformation in detail.

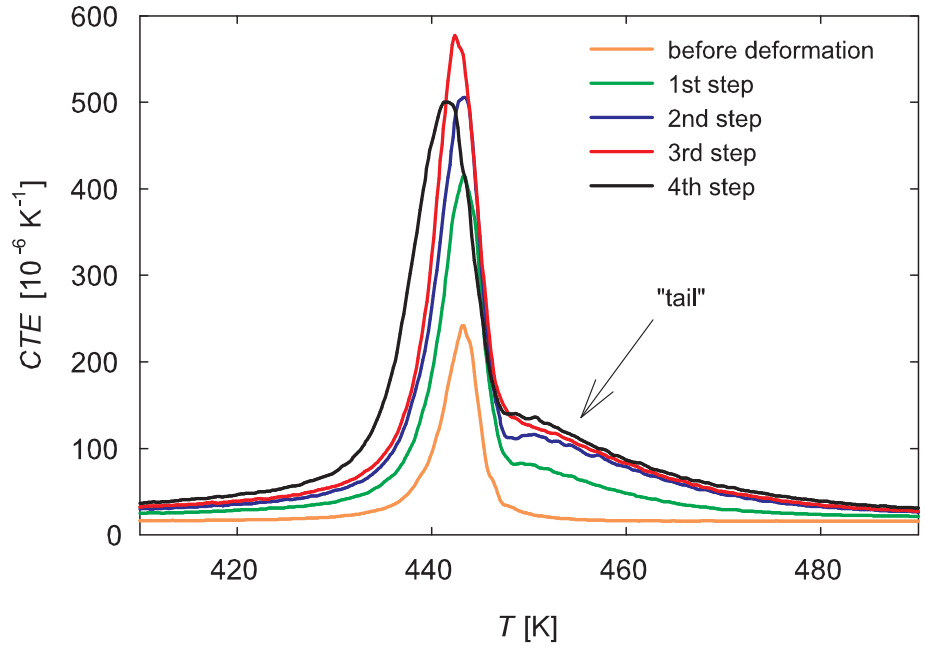

Figure 25: Temperature dependence of CTE for the cooling branch of the first thermal cycles after pre-deformation in detail.

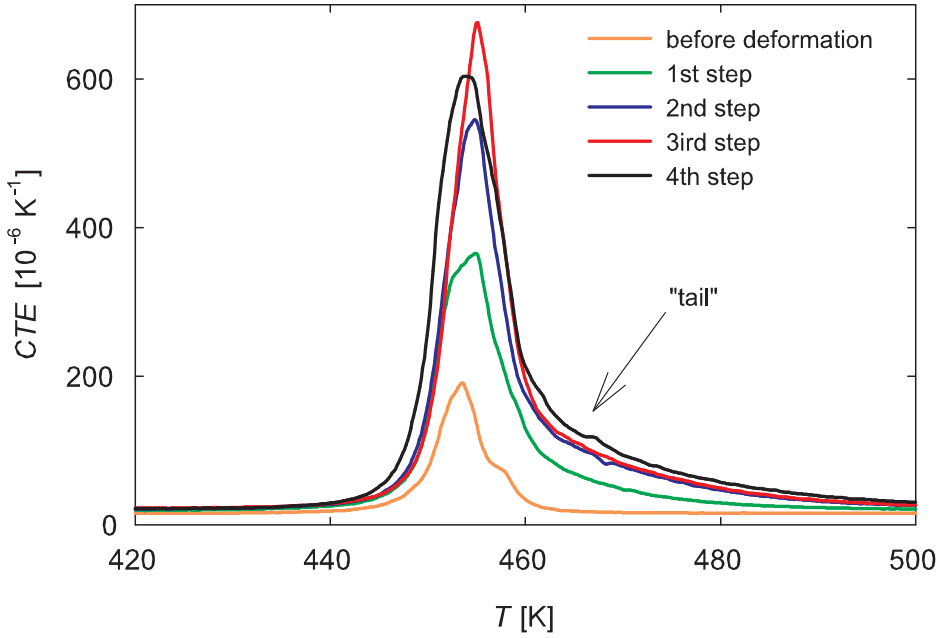

Figure 26: Temperature dependence of CTE for the heating branch of the second thermal cycles after pre-deformation in detail.

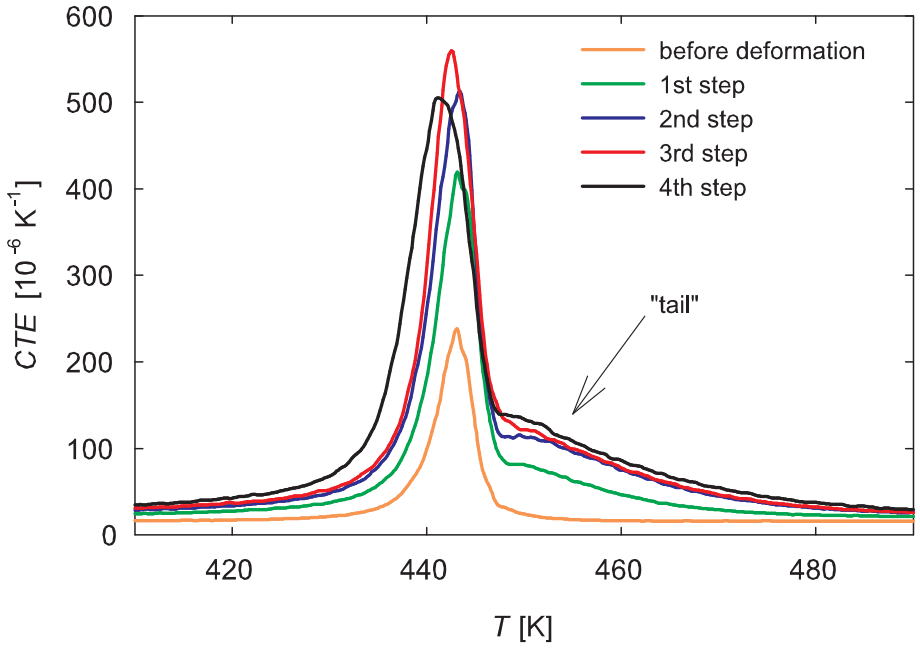

Figure 27: Temperature dependence of CTE for the cooling branch of the second thermal cycles after pre-deformation in detail.

pre-deformation step	T_{1ha} [K]	T_{1hb} [K]	T_{1c} [K]	T_{2h} [K]	T_{2c} [K]
undeformed	454	–	442	454	442
1	456	459	442	455	442
2	457	461	442	455	442
3	458	461	442	455	442
4	462	465	441	454	441

Table 3: Temperatures corresponding to the maximums of transition peaks of the temperature dependence of the CTE. Subscripts notation: 1 – the first TCAD, 2 – the second TCAD, h – heating, c – cooling, a – the first peak of the double-peak, b – the second peak of the double-peak.

For the first thermal cycles after pre-deformation, the temperature dependence of CTE in the range 420–500 K for heating and 410–490 K for cooling are depicted in figure 24 and 25, respectively. The same temperature ranges for the second thermal cycles after deformation can be seen in figures 26 and 27. Two overlapping peaks are shaped in the first thermal cycles after pre-deformation during heating. The corresponding temperatures for maximum of these peaks increase with increasing number of pre-deformation step, see table 3. Moreover, serration is observed after these two peaks in the heating branch. Both effects are more pronounced as the deformation strain is increased. The temperature dependence of CTE during cooling is "nearly the same" for the first and the second thermal cycle after each pre-deformation step.

The initial temperatures for both forward and reverse phase transformation are not affected by thermomechanical loading, whereas termination temperatures slightly shift to higher values during heating and lower values during cooling. Furthermore, "tails" of increased CTE occur at temperatures just above the temperature corresponding to the main peaks in all cases; they are marked by arrows in figures 24–27.

3.4 Thermal Diffusivity and Thermal Conductivity

The temperature dependence of thermal diffusivity of the sample was measured for several distances between the pulse generator and the sample. The relative distance was chosen to be equal to 1 when the optimal experimental conditions were achieved. This distance is termed reference distance (RD) below.

The temperature dependence of thermal diffusivity for the RD and relative distance 1.04 (1.04-distance) are shown in figure 28. The results are similar: a slight decrease of the thermal diffusivity at about 360 K and an increase of it at about 450 K can be seen. The increase indicates the MT in the sample.

In figure 29 the temperature dependence of thermal diffusivity in the martensitic temperature range (up to 440 K) for the RD are in detail. The influence of the generator–sample distance to experimental results can be seen in figure 30 for several temperatures.

In both austenitic and martensitic temperature range a linear temperature dependence of thermal diffusivity was assumed. Coefficients of this linear dependence were obtained by linear regression (the data near the magnetic transition were left out). The result for the martensitic temperature range (except the magnetic transition temperature range) is

$$\kappa(T)\,[10^{-6}\cdot \mathrm{m^2 s^{-1}}] = 2.485 + 0.001\cdot T[K]$$

in the austenitic temperature range the result is

$$\kappa(T)\,[10^{-6}\cdot \mathrm{m^2 s^{-1}}] = 3.044 + 0.003\cdot T[K]$$

The Neumann-Kopp rule was used for computing the mass specific heat capacity of studied alloy. Values of molar specific heat capacity and molar mass at room temperature (denoted by $^{\mathrm{RT}}$) can be found in [27], for instance, thus

$$C_p^{\mathrm{RT}} = 432\,\mathrm{J kg^{-1} K^{-1}}\,.$$

Measured density of the studied alloy at room temperature:

$$\varrho^{\mathrm{RT}} = (8120 \pm 10)\ \mathrm{kg\,m^{-3}}, \tag{22}$$

and the maximum rear surface temperature rise at room temperature:

$$\Delta T_{\mathrm{M}}^{\mathrm{RT}} = (1.5 \pm 0.2)\,K. \tag{23}$$

These values and equation (20) imply

$$\frac{Q}{d} = \varrho^{\mathrm{RT}} C_p^{\mathrm{RT}} \Delta T_{\mathrm{M}}^{\mathrm{RT}} = (5.3 \pm 0.7)\cdot 10^6\,\mathrm{J m^{-3}} \tag{24}$$

for the reference distance between the pulse generator and the sample at room temperature.

The maximum rear face temperature rise and effective temperature of the sample in all measurements was determined from the thermocouple records:

$$\textit{in all cases:}\quad \Delta T_{\mathrm{M}} \le 2.5\,\mathrm{K} \quad \overset{(19)}{\Longrightarrow} \quad T_{\mathrm{ef}} - T_{\mathrm{amb}} \le 4\,\mathrm{K}.$$

Using equation (21) and result (24) it is possible to determine the temperature dependence of thermal conductivity. The results are in figure 31. The linear regression of thermal conductivity both in martensitic and austenitic temperature range are marked with a red line.

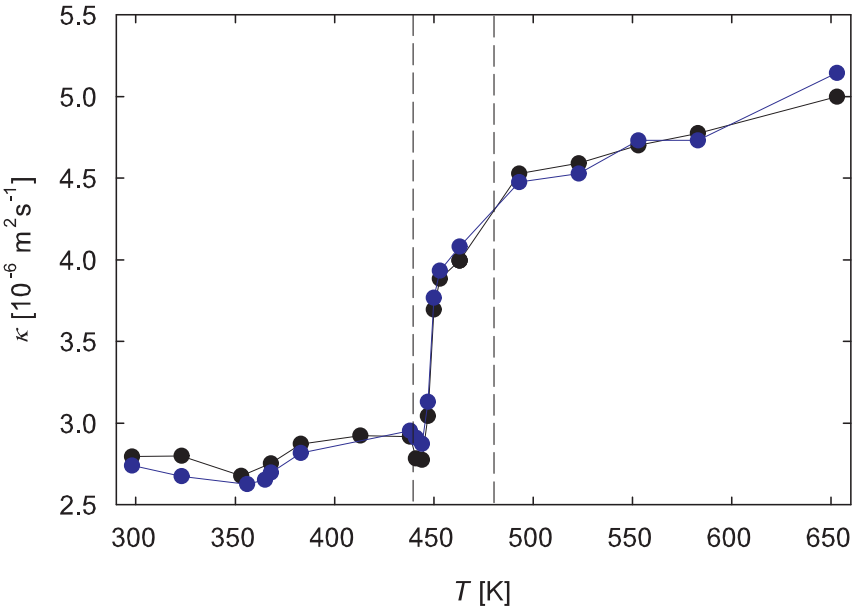

Figure 28: Temperature dependence of the thermal diffusivity of the sample. Values for reference distance/1.04-distance between the pulse generator and the sample are denoted by black/blue circles. Transient range is bounded by dashed lines.

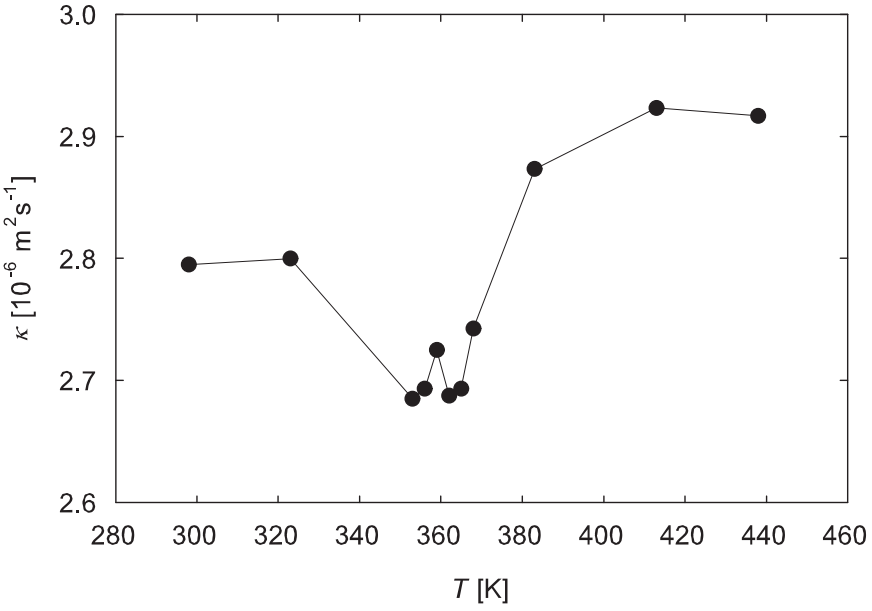

Figure 29: Temperature dependence of the thermal diffusivity in the martensitic temperature range for the reference distance between the pulse generator and the sample in detail.

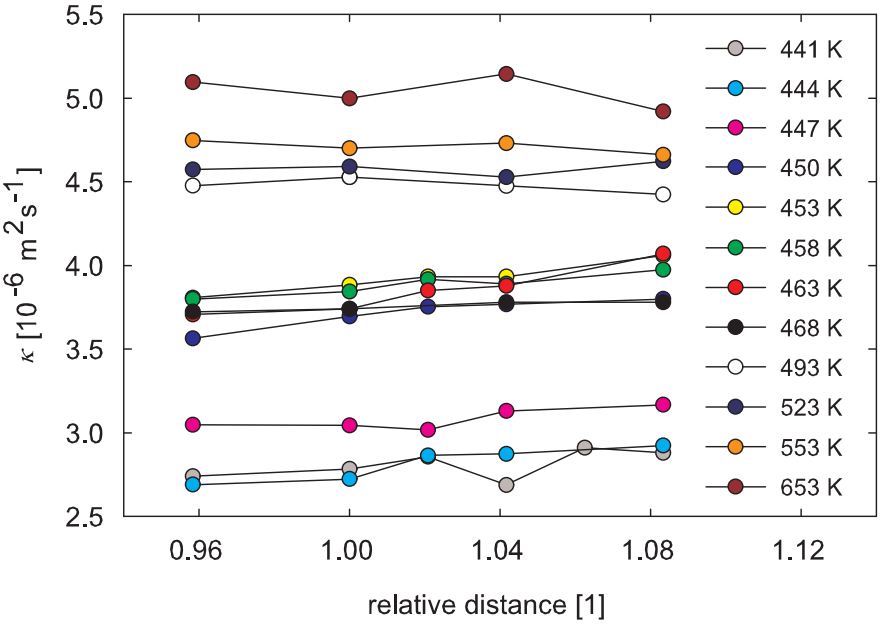

Figure 30: Thermal diffusivity of the sample for several generator–sample distances at various temperatures.

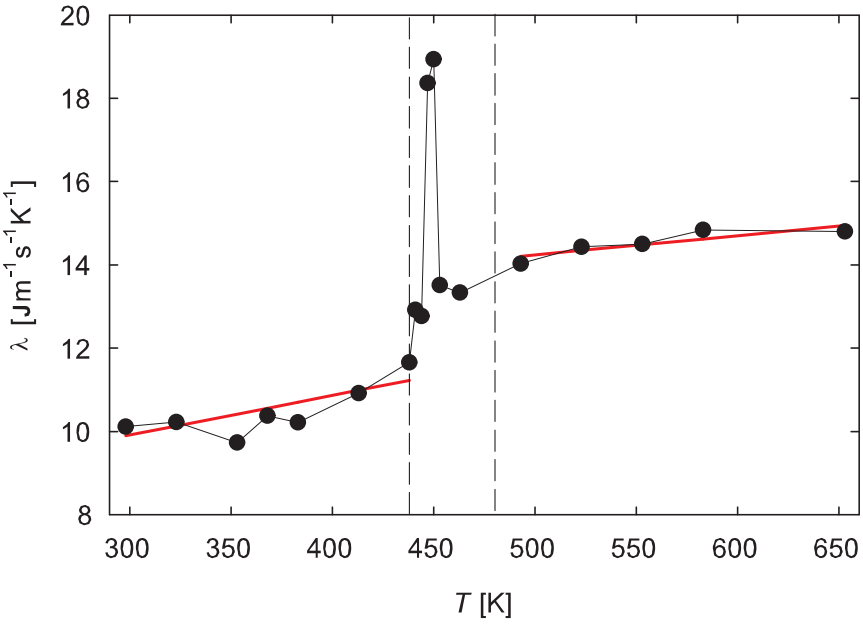

Figure 31: Temperature dependence of the thermal conductivity for the reference distance between the pulse generator and the sample. Transient range is bounded by dashed lines.

In the martensitic range linear regression implies

$$\lambda(T)\,[\mathrm{Jm^{-1}s^{-1}K^{-1}}] = 7.06 + 0.01 \cdot T[K],$$

in the austenitic temperature range the result is

$$\lambda(T)\,[\mathrm{Jm^{-1}s^{-1}K^{-1}}] = 11.932 + 0.005 \cdot T[K].$$

4 Discussion

Fig. 4 shows that two solidification processes take place in the alloy during casting. Due to temperature gradient the columnar grains grow from the wall of the mold to the center, whereas the equiaxed grains grow in the undercooled liquid in the center of the mold ahead to the columnar dendrites. The columnar front is blocked by equiaxed grains finally. Thus, different crystal structures in the ingot are a consequence of different temperature gradients and stress fields coming from different possibilities of volume changes in both the central and periphery parts of the ingot. The deviation of the crystallographic orientation of the columnar grains is usually small [21].

The MT may be influenced by the high internal stresses connected with the solidification process; particularly, when the volume changes from liquid to solid. These internal stresses and related strains and other non-equilibrium states of the as cast alloy are removed by the heat treatment. Figure 32 shows that the phase transition from austenite to martensite occurs under different conditions in equiaxed and columnar structures. The relative elongation of the alloy with the columnar structure changes by a drop in the temperature range of the phase transition. This is due to presence of preferential martensitic variants in the columnar structure formed during the solidification process (the columnar structure has the preferential crystallographic orientation perpendicular to the longitudinal axis of the sample). Similar but very small change of the relative elongation of the alloy are found for equiaxed structure, since the equiaxed structure has no preferential crystallographic orientation in the longitudinal axis of the sample [20, 28].

4.1 Dilatometry – Undeformed Sample

Three temperature subregions can be distinguished in the temperature dependence of dilatation characteristics of studied alloy.

- from 300 K to $\sim$ 420 K – martensitic temperature range
- from $\sim$ 420 K to $\sim$ 480 K – transient temperature range
- from $\sim$ 480 K to 650 K – austenitic temperature range

In the austenitic temperature range the CTE slightly increases as it is usual for common metallic alloys.

In the transient temperature range the dilatation characteristics change abruptly (step-like change of the temperature dependence of the RE, peaks of the temperature dependence of the CTE). These changes indicate the MT.

The studied alloy can be classified as a high-temperature Ni-Mn-Ga-based SMA since the magnetic phase transition precedes the martensite transition. As has been shown in many works (*e.g.* [29, 30]), the electron concentration is a useful parameter for determination of some basic properties of Ni-Mn-Ga-based alloys.

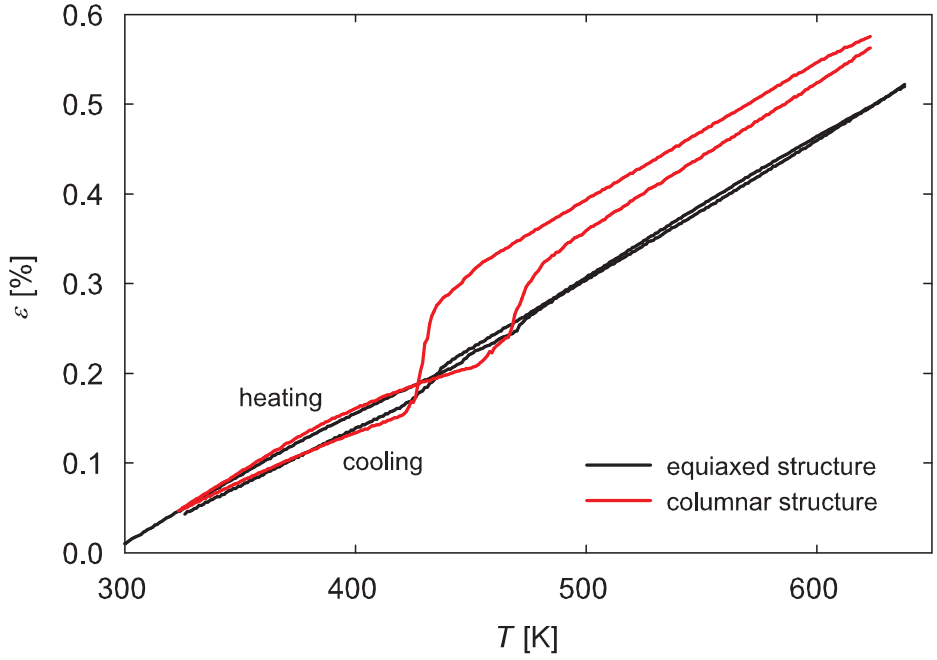

Figure 32: Comparison of the temperature dependence of the RE for equiaxed and columnar structure. Reprinted from [31].

Electron concentration, e/a, is calculated assuming the following configurations of the valence electrons and their number per atom (in brackets): for Ni: core $+3d^8\ 4s^2$ (10); for Mn: core $+3d^5\ 4s^2$ (7); for Ga: core $+4s^2\ 4p^1$ (3). These configurations correspond to the periodic table and are commonly used in band calculations of the electron structures for the Heusler alloys. For the stoichiometric composition Ni_2MnGa: $e/a = 7.5$, for composition $Ni_{53.6}Mn_{27.1}Ga_{19.3}$ studied in this work: $e/a \doteq 7.84$.

In the case of MT in the high-temperature Ni-Mn-Ga based SMAs the transition temperatures linearly increase with increasing electron concentration with the proportionality coefficient about 520 K for the increment of 1 electron per atom [30]. The result $M_s = 446\,K$ was found for an alloy $Ni_{51.2}Mn_{31.1}Ga_{17.7}$ with $e/a = 7.83$ in work [30], thus the expected value of M_s is about 451 K for the alloy studied in my thesis. Concerning figure 8, I can estimate M_s to be in the range (450 ± 3) K. Comparing this values one can see a good correspondence between performed measurements and data expected from the results in the literature.

Figures 7 and 8 reveal the influence of heating/coling rate to the transformation kinetics of the MT. The higher the heating/cooling rate is, the wider the hysteretic loop is and the more shuffled are the CTE peaks. The effect of heating/cooling rate on the transformation temperatures in TiNiCu SMA by differential scanning

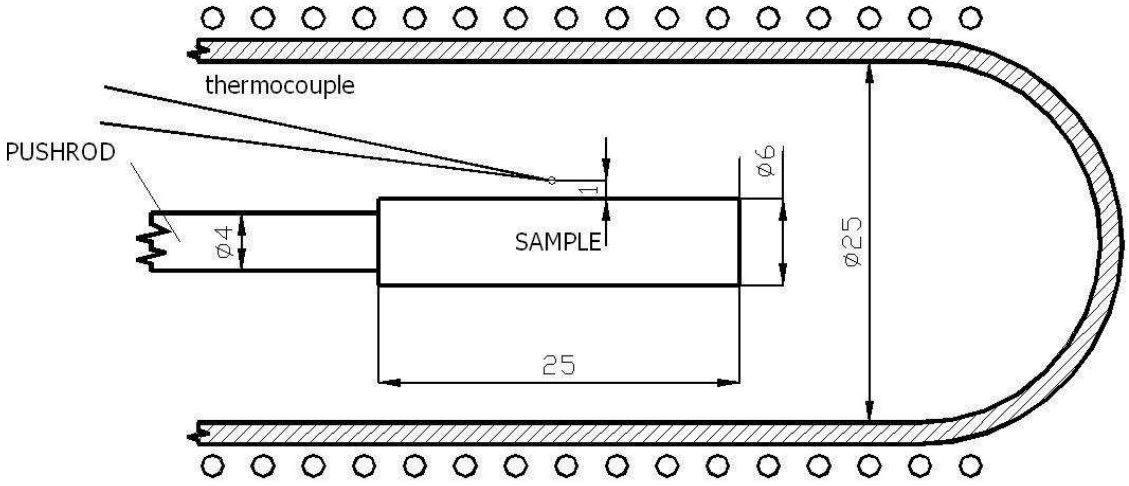

Figure 33: Schematic sketch of used dilatometer. Values in mm. Courtesy of P. Košina.

calorimetry was studied by Wang *et. al* in [32]. M_f decreased and A_f increased with increasing heating/cooling rate, whereas M_s and A_s were not sensitive to the cooling/heating rate. This behavior was explained by irradiation induced changes of the vacancy density and the chemical ordering of the crystal structures. However, results in fig. 8 are different: initialization and termination temperatures of martensite to austenite transition increase, whereas they decrease for reverse transformation (see shifted transformation loops in 7). Therefore, I assume these effects have different origin – they could be due to experimental method and setup.

The arrangement of a sample and a thermometer inside the dilatometer is shown in fig. 33. The the bulk sample is placed in the center of the furnace, the thermometer near its surface. (They must not touch each other because of the possible alloying.) Due to thermal conductivity effects, the temperature decreases from the furnace walls to the center of the sample during heating. Thus, detected values of the temperature can differ from the temperature inside the sample. The temperature of the thermometer increases more quickly than the temperature of the sample. The difference is more significant for higher heating/cooling rate.

In figure 34 the time dependence of the temperature of the thermometer for measurement of a pure platinum sample and the studied sample are shown. The latent heat spent by the martensitic phase transition occurring in Ni-Mn-Ga-based alloy causes that the rise of temperature of the thermometer for the measurement on SMAs is retarded in comparison to measurement on the platinum sample for some time. The reverse process, *i.e.* a warming of the thermometer, is detected at cooling. Inside a bulk sample the temperature increase or decrease is retarded even more.

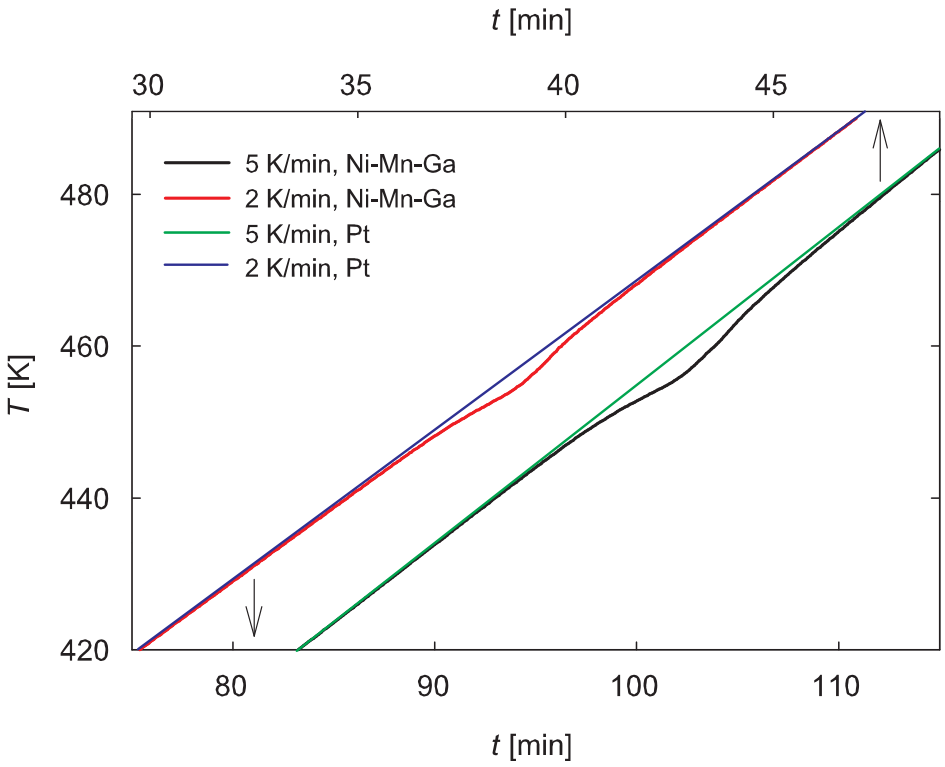

Figure 34: Time dependence of temperature of the thermometer for the studied sample and a platinum sample of the same dimensions at two heating/cooling rates.

The former facts explain the widening of the hysteretic curves in fig. 7 and related shuffling of CTE peaks in fig. 8. In that picture the temperature range of the transformation process becomes wider and the main peak of the CTE becomes lower with increasing heating/cooling rate, but the whole area under the peaks is approximately constant. It means the total amount of transformed material does not change as would be expected.

In the martensitic temperature range an anomalous behavior of the CTE was found (see fig. 9). Up to approximately 360 K the CTE of martensite increases with increasing temperature as it is usual for metallic alloys. However, an anomalous decrease of the CTE occurs in the temperature range about 360–400 K in the sample. The transient temperature of the ferromagnetic martensite to paramagnetic martensite was found to be 371 K by the measurement of the temperature dependence of the magnetization (see author's previous work [28]). The decrease could be related to the magnetic phase transition. This intriguing effect is a subject of further research.

4.2 Deformation

The stress-strain curves of four pre-deformation steps in figures 10–13 have the pseudoplasticity character. The stress-strain development in these figures is analogous to the development of stress-strain dependency measured on $Ni_{54}Mn_{25}Ga_{21}$ high-temperature polycrystalline SMA by Li *et al.* in [33]. The initial deformation stage is denoted by the red line in these figures. This stage terminates at the critical stress σ_c (see table 2), after which reorientation and plastic processes occur. The initial stage exhibits a stress plateau, which usually appears during reorientation in a deformation of a Ni–Mn–Ga-based single crystal (see [34], for instance). The critical stress in the next step is greater then in the previous one in all pre-deformation steps. The values σ_c are comparable with that of the polycrystal studied by Li *et al.* After the maximum stress, σ_{max}, is reached the sample is unloaded. The final deformation strain, ε_{def}, remains in the alloy after unloading.

In the above mentioned work Li *et al.* term the initial stage of deformation as elastic. The critical stress is considered to correspond to the starting point of the reorientation of martensite. The slope of the elastic part of loading is different from the slope of the initial part of unloading stage of the stress-strain curve, which is not discussed there.

The same asymmetry of slopes during initial stage and unloading is observed in my experiments – the unloading slope is approximately two- to three-times steeper. A possible explanation for this observation is that the reorientation process is also involved in the initial stage to some extent. During the elastic stage the material seems to be softer, because a part of strain is due to gradual reorientation.

4.3 Dilatometry – Pre-Deformed Sample

The following effect were observed in the dilatation characteristics of pre-deformed alloy in the chapter 3:

1. A part of compression strain releases in the first TCAD.
2. A part of compression strain is stored in the sample – two-way shape memory occurs.
3. "Teeth" in the temperature dependence of residual strain and peaks in the temperature dependence of stored strain occur.
4. The transformation peak of the heating branch of the first TCAD is split into two overlapping peaks.
5. Transformation temperatures of the double-peak of the heating branch of the first TCAD shift with increasing maximum deformation stress.
6. "Tails" of increased CTE occur at temperatures just above the main transformation peaks in all TCAD.
7. Serration is observed after double-peak in the heating branch of the first TCAD.

To explain the effects 1 and 2, I assume the one-way shape memory effect (OWSME), the two-way shape memory effect (TWSME) and a partial recovery appear in the first thermal cycle after the pre-deformation, whereas only the TWSME and a negligible thermal recovery appear in the second and following thermal cycles after deformation. Thus, to distinguish each contribution the residual and stored strain were determined as described in section 3.3).

Concerning the evolution of the total strain of the sample during deformation and thermal cycles summarized in figures 20 and 21, I can suggest an explanation of the length changes of the sample in each step of performed mechanical and thermal loading experiments as following.

First, the sample is deformed to the maximum strain, $\varepsilon_{\max}$. Since the reorientation process (detwinning, increase of preferential variants fraction) and plastic deformation (dislocation creation and their movement) are involved during loading, a non-zero strain, $\varepsilon_{\mathrm{def}}$, remains in the sample after unloading.

During the first thermal cycles after pre-deformation a part of induced deformation strain is released. This is easy to see in figure 14, where the value of the RE after the thermal cycle is higher than at the beginning of the cycle (compare with the cycle before deformation). This released strain is termed residual strain, it was determined as it is described in chapter 3 and it is depicted in figures 16–19 for each cycle. A part of the released residual strain at the end of the first TCAD could be a consequence of thermal recovery in the alloy (due to increased temperature), but the most important involved effect is the OWSME – during heating the oriented preferential martensitic variants transformed to austenite and twinned variants were formed during cooling with contraction of the sample as a result. Therefore, the value of released strain after the first TCAD is affected only by the most prior deformation step, not the whole thermomechanical history of the sample.

The value of the OWSME depends on the total amount of martensitic variants preferentially oriented by the pre-deformation. Since I assume the martensite is continuously reoriented during the whole loading stage, especially after the critical stress is reached, this amount should be related to the maximum deformation strain. This is in agreement with results in figure 21, where the relation between the residual strain and the maximum deformation strain can be seen.

After the second thermal cycles after the pre-deformation only a negligible part of imposed strain is released probably due to recovery, see the negligible difference of the RE after the thermal cycle in fig. 15. Thus, the final strain of the sample after the second thermal cycle, ε_2, is approximately equal to the final strain of the sample after the first thermal cycle, ε_1. However, the reversible strain, manifested by the loops in the figure, occurs. The increase of this reversible strain after a deformation step is termed stored strain. Stored strain was calculated and depicted in figures 16–19 for each cycle. The reversible change in length of the sample due to stored strain is two-shape memory effect. The total value of stored strain, $\varepsilon_{\mathrm{TW}}$, depends

on the whole thermomechanical history of the sample.

In contrast to the OWSME, the value of the TWSME is related to permanent internal stress fields stored in the sample. They are of various origins. The critical stress could be a measure of intensity of internal stress fields in a deformation step, since σ_c indicates the amount of external stress needed to initiate the reorientation process. The higher the absolute value of the critical stress is, the higher internal stress fields are in the sample and the higher value of the TWSME, ε_{TW}, can be obtained after deformation as depicted in figure 21.

Figure 20 shows that with increasing maximum deformation strain up to absolute value of 3.8% the final strain after the second TCAD, ε_2, seems to attain saturation value about -1.5%. This implies the value of the total reversible strain (elasticity and OWSME) is about -2.3%. It can also mean the internal structure is stabilized and only small plastic deformation is involved in the last deformation step. In other words, the sample was trained [35].

Let us concern the development of the CTE next. The high intensity of the CTE heating peaks in fig. 22 shows a large length change of the sample during heating in the first TCAD. The very small variation in behavior of the alloy in the cooling branch of the second thermal cycle with respect to the cooling branch of the first thermal cycle confirms steady behavior after the first heating of deformed martensite to the maximum studied temperature as I supposed in the previous section.

The shift of transformation peaks in the heating branch of the first TCAD mentioned as effect 5, was already observed by Gao *et al.* in [36]. The following explanation was suggested:

- Considerable damage of the interfacial coherence of martensitic variants after deformation of martensite was observed by transmission electron microscopy. During the deformation some kind of the locked-in microstructure or microquasi-plastic deformation, etc., were supposed to be generated. These microstructure would require higher driving force in subsequent transformation process, resulting in the increase of the martensite to austenite transformation temperature.
- With increasing deformation, more lattice defects were generated inside the variants as well as in the interfacial boundaries between variants. Although the dislocations introduced by the compression deformation might be inherited by the parent phase, there were no remarkable influence of the dislocations on the transformation temperatures, which was attributed to the large grain size of the Ni–Mn–Ga alloy.

Using my results I attempt to quantify the influence of pre-deformation to the shift of the martensite to austenite transition temperatures.

Let us assume deformation imposed internal stresses of various origin (locked-in microstructure or microquasi-plastic deformation) occur in the sample after unloading in a pre-deformation step as proposed by Gao *et al.*. These deformation

imposed stresses retard the transformation kinetics of the martensite to austenite transition, but they can release during the transition and they do not influence the subsequent transitions. Let us suppose the increase of the deformation imposed stresses is equal to the increase of the maximum deformation stress, as the increase of the maximum stress can induce formation of new locked-in microstructures or increase of the microquasi-plastic deformation. Finally, let us assume the transformation temperature shift is correlated to deformation imposed stresses through the Clausius-Clapeyron equation (see chapter 1).

To determine the correlation between the maximum deformation stress and the temperatures of transformation peaks I use the linear regression. The linear regression of temperatures corresponding to the first peak in the heating branch of the first TCAD, $T_{1\mathrm{ha}}$, and the maximum deformation stresses in the previous pre-deformation step, $\sigma_{\max}$, implies the value of critical slope $s := \mathrm{d}\sigma/\mathrm{d}T$ (see equation 4)

$$s_1 = (-13.3 \pm 1.6)\,\mathrm{MPa\,K^{-1}}.$$

The value of this parameter for the second peak in the heating branch of the first TCAD, $T_{1\mathrm{hb}}$, and the maximum deformation stresses in the previous pre-deformation step is

$$s_2 = (-14.1 \pm 0.3)\,\mathrm{MPa\,K^{-1}}.$$

In the literature (e.g. [37,38]), the typical values of s vary in the range from -7 to $-14\,\mathrm{MPa\,K^{-1}}$ for compression (depends on chemical composition). Obviously, the values determined from my results are in the this value range with respect to standard error.

The temperature shift of the first peak in the heating branch for the undeformed sample and the same sample after the first deformation step is 2 K. The values of parameter s imply the internal stress of the undeformed sample is about $-120\,\mathrm{MPa}$. This value can be explained as a minimum deformation needed to initiate the initialization of microquasi-plastic deformation or locked-in microstructure forming in the martensite.

The shift of transformation temperatures is the source of the effect 3 – the "tooth" in the temperature dependence of residual strain in figures 16–19. As the transformation temperature A_s shifts the difference suddenly drops. Thus, the width of the "tooth" is proportional to the temperature shift. The small peaks in the temperature dependence of the stored strain are of the same origin. Since the shift in transformation temperatures is much smaller than in previous case, the effect is also much smaller.

Although effects similar to 4, 6 and 7 are observed in results of other thermal methods (*e.g.* differential scanning calorimetry [38]), they have not been unambiguously clarified in the literature yet. Further research is planned to clarify the inner mechanism of these effects.

4.4 Thermal Diffusivity and Thermal Conductivity

As mentioned above, the material undergoes a first order solid-to-solid martensitic phase transformation in temperature range 440–490 K. Moreover, due to magnetic measurements a second order ferromagnetic phase transition occurs at temperatures about 370 K. These facts are confirmed, thermal diffusivity sharply changes in the transient range and decreases near temperature 370 K, see figures 28 and 29. In martensitic and austenitic temperature ranges thermal diffusivity slightly increases except for temperatures near the ferromagnetic phase transition. Diffusivity increases with increasing temperature faster for austenite than for martensite.

Figure 30 shows the thermal diffusivity results are almost independent on generator–sample distance with respect to experimental errors, which demonstrates the accuracy of the method and measuring apparatus.

The thermal conductivity determined as a product of the thermal diffusivity, density and the specific heat is shown in 31. Again, three temperature regions can be seen on this temperature dependence. The thermal conductivity in both martensitic and austenitic temperature range increases. In the transition temperature range a peak occurs as a consequence of the peak on the temperature dependence of the specific heat. However, this peak has no physical sense because the heat conduction equation used for the flash method is solved on condition that no phase transformation occurs in the material.

The coefficient of thermal conductivity of Ni_2MnGa was measured by Kuo *et al.* with a direct heat-pulse technique (see [39]). The resulting value was approximately $15\,\mathrm{Jm^{-1}s^{-1}K^{-1}}$ at room temperature. However, Ni_2MnGa alloy is in the ferromagnetic austenitic state at room temperature, whereas the alloy studied in this work is in the paramagnetic martensitic state at room temperature. Due to my results, the measured value of the thermal conductivity of $Ni_{53.6}Mn_{27.1}Ga_{19.3}$ alloy is $14 - 15\,\mathrm{Jm^{-1}s^{-1}K^{-1}}$ in the austenitic temperature range (480–650 K). Thus, both measurements are in good agreement.

5 Conclusions

- The relative elongation (RE) and the linear coefficient of thermal expansion (CTE) of undeformed and compression pre-deformed polycrystalline samples of $Ni_{53.6}Mn_{27.1}Ga_{19.3}$ shape memory alloy with columnar grains were studied in the temperature range 300–650 K. Due to martensitic transformation occurring in the alloy the studied temperature range was divided into three regions: martensitic (300–420 K), transient (420–480 K) and austenitic(480–650 K).
- In the case of undeformed sample the analysis of results concerned on the influence of heating/cooling rate to measured transient temperatures. Because of the experimental setup the temperature of the thermometer differs from the temperature inside the sample. It was also found the latent heat of the phase transition influences the temperature measured by the thermometer. These facts lead to an artificial widening of the hysteresis loop in the temperature dependence of the RE and to a shift of transformation peaks in the temperature dependence of the CTE.
- The studied alloy was pre-deformed in compression in four steps up to final strain of -3.8% at room temperature. The stress-strain behavior of each step was analyzed. The initial elastic stage finished at the critical stress after which reorientation process occurred. After full unloading a deformation induced strain remained in the alloy.
- After each deformation step two thermal cycles were performed. A part of the deformation induced strain released in the first thermal cycle after deformation (first TCAD) – the one-way shape memory effect (OWSME) occurred. The amount of strain released during the OWSME was related to the maximum deformation strain. Negligible part of the deformation induced strain released in the second TCAD. The accumulation of irreversible stored strain after each deformation increased the two-way shape memory effect (TWSME) in the sample as well as the critical reorientation stress. The final strain of the sample after two thermal cycles seemed to attain saturation value.
- The observed shift of transformation peaks in the temperature dependence of the CTE was related to deformation imposed internal stress as proposed by Gao et al. in [36]. The value of the internal stress, which releases after heating of the sample in the first TCAD, was related to the maximum deformation stress and the Clausius-Clapeyron equation was used to estimate the value of critical transformation slope. The obtained results are compared with values in the literature.

- Other deformation induced effects observed in the temperature dependence of the CTE are: splitting of the transformation peak of the heating branch of the first TCAD into two overlapping peaks, "tails" of increased CTE occurring at temperatures just above those of the main transformation peaks in all TCAD, serration of this tail in the heating branch of the first TCAD. These effects have not been unambiguously clarified in the literature yet, thus, they are objects of further research.
- The thermal diffusivity of the studied shape memory alloy was measured by the flash method, the thermal conductivity was determined and compared with results in the literature.

Index

Bibliography

[1] Roytburd, A. L.: *Kurdjumov and His School in Martensite of the 20th Century*, Mat. Sci. Eng. A **273–275** (1999), 1–10.

[2] Bekker, A., Brinson, L. C.: *Temperature-Induced Phase Transformation in a Shape Memory Alloy: Phase Diagram Based Kinetics Approach*, J. Mech. Phys. Solids **45** (1997), 949–988.

[3] Porter, D. A., Easterling, K. E.: *Phase Transformations in Metals and Alloys*, CRC Press, Cheltenham, 2001.

[4] Enkovaara, J., Ayuela, A., Zayak, A. T., Entel, P., Nordström, L., Dube, M., Jalkanen, J., Impola, J., Nieminen, R., M.: *Magnetically Driven Shape Memory Alloys*, Mat. Sci. Eng. A **378** (2004), 52–60.

[5] Ge, Y.: *The Crystal And Magnetic Microstructure Of Ni-Mn-Ga Alloys*, Doctoral Thesis, Helsinki University of Technology, 2007.

[6] Ford, D. S., White, S. R.: *Thermomechanical Behavior of 55Ni45Ti NITINOL*, Acta Mater. **44** (1996), 2295–2307.

[7] Frost, M.: *Elastic properties of blood veins with a scaffold*, Diploma Thesis, Charles University in Prague, 2007.

[8] `http://www.fzu.cz/departments/metals/sma/brana_cz/index.php`

[9] Ortín, J.: *Preisach Modeling of Hysteresis for Pseudoelastic Cu-Zn-Al Single Crystal*, J. Appl. Phys. **71** (1992), 1454–1461.

[10] Šittner, P., Takakura, M., Tokuda, M.: *Shape Memory Effects Under Combined Forces*, Mat. Sci. Eng. A **234–236** (1997), 216–219.

[11] Wang, J. J., Omori, T., Sutou, Y., Kainuma, R., Ishida, K.: *Two-way Shape Memory Effect Induced by Cold-Rolling in Ti–Ni and Ti–Ni–Fe Alloys*, Scripta Mater. **52** (2005), 311—316.

[12] `http://www.riken.jp/lab-www/nanomag/research/heusler_e.html`

[13] Söderberg, O., Aaltio, I., Ge, Y., Heczko, O., Hannula, S.-P.: *Ni–Mn–Ga Multifunctional Compounds* Mat. Sci. Eng. A **481-482** (2008), 80–85.

[14] Jiang, C., Feng, G., Gong, S., Xu, H.: *Effect of Ni Excess on Phase Transformation Temperatures of Ni-Mn-Ga Alloys*, Mat. Sci. Eng. A **342** (2003), 231–235.

[15] Chernenko, V. A., Cesari, E., Kokorin, V. V., Vitenko, I. N.: *The Devolopment of New Ferromagnetic Shape Memory Alloys in Ni-Mn-Ga System*, Scripta Metall. Mater. **33** (1995), 1239–1244.

[16] Jiang, C., Muhammad, Y., Deng, L., Wu, W., Xu, H.: *Composition Dependence on the Martensitic Structures of the Mn-rich Ni-Mn-Ga Alloys*, Acta Mater. **52** (2004), 2779–2785.

[17] Pons, J., Chernenko, V. A., Santamarta, R., Cesari, E.: *Crystal Structure of Martensitic Phases in Ni-Mn-Ga Shape Memory Alloys*, Acta Mater. **48** (2000), 3027–3038.

[18] Seguí, C., Chernenko, V. A., Pons, J., Cesari, E., Khovailo, V., Takagi, T.: *Low Temperature-Induced Intermartensitic phase Transformations in Ni-Mn-Ga Single Crystal*, Acta Mater. **53** (2005), 111–120.

[19] Ullakko, K., Huang, J. K., Kantner, C., O'Handley, R. C., Kokorin, V. V.: *Large Magnetic Field-Induced Strains in Ni_2MnGa Single Crystals*, Appl. Phys. Lett. **69** (1996), 1966–1968.

[20] Rudajevová, A., Frost, M., Jäger, A.: *Thermal Expansion Characteristics of $Ni_{53.6}Mn_{27.1}Ga_{19.3}$ Alloy with Columnar Structure*, Mater. Sci. Tech.-Lond. **23** (2007), 542–546.

[21] Potschke, M., Gaitzsch, U., Roth, S., Rellinghaus, B., Schultz, L.: *Preparation of Melt Textured Ni–Mn–Ga*, J. Magn. Magn. Mater. **316** (2007), 383-–385.

[22] Besseghini, S., Villa, E., Passaretti, F., Pini, M., Bonfanti, F.: *Plastic Deformation of NiMnGa Polycrystals*, Mat. Sci. Eng. A **378** (2004), 415-–418.

[23] Feng, X., Yong, L., Pagounis, E.: *Thermally Induced Fracture of Single Crystal Ni–Mn–Ga Ferromagnetic Shape Memory Alloy*, J. Alloy Compd. **415** (2006), 188-–192.

[24] Parker, W. J., Jenkins, R. J., Butler, C. P., Abbott, G. L.: *Flash Metod of Determining Thermal Diffusivity, Heat Capacity and Thermal Conductivity*, J. Appl. Phys. **32** (1961), 1679–1684.

[25] Rudajevová, A.: *Determining the Relative Radiation Absorptivity of Plasma-Sprayed $ZrSiO_4$ and Al_2O_3 Coatings*, Silikáty **33** (1989), 61–67.

[26] Taylor, R.: *Construction of Apparatus for Heat Pulse Thermal Diffusivity Measurements from 300 – 3000 K*, J. Phys. E **13** (1980), 1193–1198.

[27] Brož, J., Roskovec, V., Valouch, M.: *Fyzikální a matematické tabulky*, SNTL, Prague 1980.

[28] Frost, M.: *The Study of Dilatation Characteristics of the Shape Memory Ni_2MnGa Alloy*, Bachelor Thesis, Charles University in Prague, 2006.

[29] Schlagel, D. L., Wu,Y. L., Zhang, W., Lograsso, T. A.: *Chemical Segregation During Bulk Single Crystal Preparation of Ni–Mn–Ga Ferromagnetic Shape Memory Alloys*, J. Alloy Compd. **312** (2000), 77—85.

[30] Chernenko, V. A., Cesari, E., Kokorin, V. V., Vitenko, I. N.: *The Development Of New Ferromagnetic Shape Memory Alloys In Ni-Mn-Ga System*, Scripta Metall. Mater. **33** (1995), 1239–1244.

[31] Rudajevová, A.: *Analysis of the Thermal Expansion Characteristics of $Ni_{53.6}Mn_{27.1}Ga_{19.3}$ Alloy*, J. Alloy Compd. **430** (2007), 153–157.

[32] Wang, Z. G., Zu, X. T., Huo, Y.: *Effect of Heating/Cooling Rate on the Transformation Temperatures in TiNiCu*, Thermochim. Acta **436** (2005), 153—155.

[33] Li, Y., Xin, Y., Jiang, C., Xu, H.: *Mechanical and Shape Memory Properties of $Ni_5 4 Mn_2 5 Ga_2 1$ High-Temperature Shape Memory Alloy*, Mat. Sci. Eng. A **438-440** (2006), 978-–981.

[34] Söderberg, O., Straka, L., Novák, V., Heczko, O., Hannula, S.-P., Lindroos, V.K.: *Tensile/Compressive Behaviour of Non-Layered Tetragonal $Ni_{52.8} Mn_{25.7} Ga_{21.5}$ Alloy*, Mat. Sci. Eng. A **386** (2004), 27—33.

[35] Zhang, X. M., Fernandez, J., Guilemany, J. M.: *Role of External Applied Stress on the Two-Way Shape Memory Effect*, Mat. Sci. Eng. A **438–440** (2006), 431-–435.

[36] Gao, Z. Y., Chen, F., Cai, W., Zhao, L. C., Wu, G. H., Shen, B. G., Zhan, W. S.: *Effect of Pre-Deformation on Martensitic Transformation Behavior and the Microstructure of a Ni–Mn–Ga Alloy*, Mat. Sci. Eng. A **438–440** (2006), 974—977.

[37] Chernenko, V. A., Kokorin, V. V., Babii, 0. M., Zasimchuk, I. K.: *Phase Diagrams in the Ni-Mn-Ga System Under Compression*, Intermerallics **6** (1998), 29–34.

[38] Chernenko, V. A., Pons, J., Cesari, E., Ishikawa, K.: *Stress–Temperature Phase Diagram of a Ferromagnetic Ni–Mn–Ga Shape Memory Alloy*, Acta Mater. **53** (2005), 5071—5077.

[39] Kuo, Y. .K., Sivakumar, K. M., Chen, H. C., Su, J. H., Lue, C. S.: *Anomalous Thermal Properties of the Heusler alloy $Ni_{2+x} Mn_1 - x Ga$ near the Martensitic Transition*, Phys. Rev. B **72** (2005), 54116.